Medizinische Fakultät
der
Universität Duisburg-Essen

Aus dem Institut für Diagnostische und Interventionelle
Radiologie und Neuroradiologie

Magnetic resonance fingerprinting: Accuracy, repeatability and implementation in clinical practice

I n a u g u r a l - D i s s e r t a t i o n
zur
Erlangung des Doktorgrades der Medizin
durch die Medizinische Fakultät
der Universität Duisburg-Essen

Vorgelegt von
Dr. rer. nat. Jasmin Viktoria Jäger
aus Witten
2022

Dekan: Herr Univ.-Prof. Dr. med. J. Buer
1. Gutachter: Frau Prof. Dr. med. L. Umutlu
2. Gutachter: Herr Prof. Dr. med. K. Naßenstein

Tag der mündlichen Prüfung: 28. März 2023

Table of contents

1. Introduction 5

1.1 Motivation 5

1.2 Conventional Magnetic Resonance imaging 7

1.3 Quantitative Magnetic Resonance imaging 9

1.4 Magnetic Resonance Fingerprinting 10

1.4.1 Data acquisition, 'the fingerprint' 11

1.4.2 Dictionary generation 13

1.4.3 Pattern recognition 13

1.5 Aim of this work 14

2. Material and Methods 16

2.1 ISMRM System Phantom 16

2.2 Study population 17

2.2.1 Healthy volunteers 17

2.2.2 Patients 18

2.3 MRF implementation and acquisition parameters 18

2.4 Region of interest analysis 19

2.5 Statistical analysis 20

3. Results 22

3.1 Phantom study 22

3.2 Healthy volunteer study 27

3.2.1 T_1 and T_2 quantification in different anatomic regions 28

3.2.2 Analysis of data repeatability 31

3.3 Patient study 32

3.3.1 T_1 and T_2 quantification and repeatability 32

3.3.2 Aging progression of relaxometry data 37

4. Discussion 39

4.1 MRF validation in phantom scans 39

4.2 MRF validation in healthy volunteers 40

4.2.1 Comparison to conventional mapping techniques and initial MRF results 41

4.2.2 Discussion of data variability 42

4.3 MRF validation in patients 43

4.4 Limitations 45

4.5 Conclusion 46

5. Summary/ Zusammenfassung 47

6. Bibliography 49

7. Appendix 54

7.1 Supplemental material 54

7.1.1 Comparison of volunteer relaxometry data to conventional mapping techniques 54

7.1.2 Comparison of volunteer relaxometry data to previous MRF results 56

7.2 List of figures 57

7.3 List of tables 58

7.4 List of abbreviations 59

8. Acknowledgement 60

9. Curriculum vitae 61

1. Introduction

The aim of this thesis is to investigate the feasibility and applicability of an integration of Magnetic resonance fingerprinting (MRF) into clinical imaging workflows. The focus is put on the evaluation of the stability and reproducibility of quantitative T_1 and T_2 relaxation time measurements in an imaging phantom as well as in healthy tissue in dedicated anatomic brain regions from a volunteer and patient collective utilizing MRF. In this first chapter, the need for a fast and accurate quantitative magnetic resonance (MR) imaging technique is described including a focused discussion of current limitations in common clinical and experimental quantitative MR imaging techniques, followed by a review of the technical background of Magnetic resonance fingerprinting and recent medical applications.

1.1 Motivation

In MRI (Magnetic Resonance Imaging), tissues in the human body can be distinguished according to their unique MR parameters such as longitudinal (T_1) or transverse (T_2) relaxation times.

Since magnetic resonance techniques were introduced into clinical medicine four decades ago, MR examinations in daily clinical routine to date rely on the generation of qualitative weighted images by systematically setting distinct MR parameters such as the repetition time (TR), echo time (TE) and flip angle (FA) throughout the acquisition. These acquisition parameters are chosen to emphasize structures of interest, such as pathological areas by means of an increase of relative image intensity and contrast, respectively, in mainly T_1- or T_2-weighted images. Thereby, in the final image, a tissue is described either as ‘hyperintense’ or ‘hypointense’ compared to the surrounding area. Established MR diagnostic criteria are based on qualitative gray-scaled contrast to characterize and compare underlying pathologies to healthy structures (Grover et al. 2015). This implies that a considered tissue may display different intensities depending on factors like the type and set-up of the scanner, signal detectors and image reconstruction (Trattnig et al. 2015). As imaging parameters in MR are not measured in absolute values, an objective evaluation or isolated quantification of tissue properties is not typically accessible. Hence, over the last decades reading and reporting of MR imaging has been established based on a rather subjective, non-quantified manner, which makes MR imaging and reporting difficult to objectify and standardize.

A longtime goal in MR science has therefore been a simple, fast and absolute quantification of tissue properties to serve as noninvasive biomarkers, enable reproducibility and

comparability throughout multicentered studies in order to improve diagnosis and therapeutic assessment.

Much effort has been invested into quantitative mapping techniques that can measure absolute tissue properties such as T_1 and T_2 relaxation times. Early single-parametric approach involved the measurement of one parameter such as T_1 or T_2 mapping at a time. In contrast, multiparametric mapping techniques provide both T_1 and T_2 values within a single acquisition (Just and Thelen 1988; McSheehy et al. 2010; Ghugre et al. 2011). Unfortunately, these conventional quantitative mapping techniques suffer from reduced time efficiency and limited repeatability and reproducibility. So far, a fast and robust, fully quantitative and accurate measurement of tissue properties that may be adopted into the clinical workflow remains challenging (Badve et al. 2015; Jiang et al. 2017).

In 2013 Magnetic Resonance Fingerprinting (MRF) was introduced as a novel approach to quantitative multiparametric MR imaging providing simultaneous measurements of multiple imaging parameters in one single acquisition. In the MRF acquisition scheme, the acquisition parameters are deliberately varied in a pseudorandom manner, so that each tissue generates a unique signal response comparable to a person's fingerprint. A predefined database, the dictionary, stores pre-simulated physiologically possible signal evolutions from realistic tissue parameter combinations. A pattern recognition algorithm is used to select the dictionary entry that best represents the acquired signal evolution of each voxel analogous to a forensic fingerprinting identification process (Ma et al. 2013; Coppo et al. 2016). Recent MRF experiments have shown scan times comparable to MRI examinations used in clinical settings (Jiang et al. 2015). It has been proven to be a robust method regarding signal noise, sensitivity to system imperfections and motion. The MRF framework has been tested in various experiments assessing healthy and pathologic structures in brain, breast, liver and prostate tissue (Panda et al. 2019; Panda et al. 2017; Hsieh and Svalbe 2020). Most of the mentioned studies focus on the proof of principle of the MRF implementation and the optimization of time efficiency. Only few trials assess the repeatability and reproducibility of the MRF method that is however essential for validation and clinical application of the method (Jiang et al. 2017; Körzdorfer et al. 2019). Repeatability and reproducibility mean, that any variation in, for example, relaxometry values obtained via repetitive measurements or from different scanner systems must be smaller than the physiological differences between healthy and pathologic tissues to interpret results. So far, studies evaluating the repeatability and accuracy of in vivo MRF measurements are based on a small number of participants (Badve et al. 2015; Körzdorfer et al. 2019). The validation of normative quantitative relaxometry parameters providing

reliable reference data for accurate differentiation of pathologic structures would profit from larger cohorts of study subjects.

The study in hand puts the focus on assessment of the stability and repeatability of MRF-derived relaxometry data in an imaging phantom, various non-pathologic brain tissues in volunteers and a large patient cohort to investigate the potential of MRF for integration into routine clinical workflows. The assessment of accurate and reliable quantification of normative brain tissue parameters could contribute to the establishment of a clinical reference data base of normal relaxometry data in order to facilitate multicentered studies and improve future diagnostics in neuroimaging.

1.2 Conventional Magnetic Resonance imaging

MR imaging techniques are based on the physical phenomenon of nuclear magnetic resonance (NMR), by means of the absorption and emission of radiofrequency electromagnetic radiation by atomic nuclei subjected to a magnetic field.

The most commonly used nuclei in MRI are hydrogen nuclei, i. e. protons which occur widely in all body fluids, showing a strong magnetic response (Grover et al. 2015; Dale et al. 2015). Subjected to an external magnetic field denoted as B_0, hydrogen nuclei align along the direction of the magnetic field due to their intrinsic spin. Because of random interactions between the nuclei, this alignment is only partial. The sum of all spin directions creates a net (total) magnetization M. The minimal angular deviations of the spin axes from B_0 lead to a precessional motion of M at a constant rate around the axis of B_0. The precession frequency depends on the strength of the external field and is expressed by the Larmor equation $\omega_L = \gamma B_0$, with ω_L denoting the Larmor-frequency of spin precession.

When electromagnetic radiation, usually termed as short radiofrequency (RF) pulses is applied, the interaction of the magnetic part B_1 of the electromagnetic wave leads to a transition of the spins from lower to higher energy levels. Described by a simplified vector model, M is tilted out of its equilibrium position and relaxes back to its state of equilibrium, once the RF pulse is turned off. The short RF pulses of microsecond duration contain several frequencies at a narrow bandwidth. The energy that is emitted during the relaxation process by the spins induces a voltage that is recorded by a receiver coil. This nuclear induction voltage is termed as the free induction decay (FID). Practically, multiple FIDs are observed and averaged applying several RF pulses to improve the signal-to-noise ratio (SNR) (Lugauer and Wetzl 2018).

The relaxation process of nuclear spins to the thermal equilibrium state is characterized by a longitudinal and a transverse relaxation time. The longitudinal relaxation time T_1 defines the time required for the z-component of M (M_z) to return (i. e. recover) to its initial direction parallel to B_0. This process is associated with energy transfer to the surrounding nuclei and called spin-lattice relaxation. The transverse or T_2 relaxation time characterizes the decay or dephasing of the transverse components of magnetization M_{xy} towards its equilibrium value. The dephasing of spins mainly results from local magnetic field fluctuations that are particularly effective between spins of the same kind or spin-spin-relaxation.

The longitudinal and transverse relaxation process is tissue specific. Cerebral spinal fluid for example contains a high amount of water and shows long T_1 and T_2 times compared to dense tissue like white or gray matter where T_1 recovery and T_2 decay is faster leading to shorter T_1 and T_2 values. In total, T_1 values in the human brain usually range from 200 to 2000 ms, whereas T_2 values range from 20 to 500 ms at a temperature of 37°C (Dougherty et al. 2004). These variations of T_1 and T_2 times create the differences in tissue contrast on MR images (Bojorquez et al. 2017; Weishaupt et al. 2014).

Two key parameters termed as the repetition time TR and the echo time TE are used to emphasize a certain type of tissue contrast in MR images depending on the applied sequence. The conventional MR signal is acquired by applying repetitive RF pulses and measurement of the resulting FID at specific time-points. During the repeating series of RF pulses the time length between two consecutive RF pulses is termed as the repetition time TR. The echo time TE is the time range between the RF pulse application and the peak of the MR signal induced in the receiver coil (Bitar et al. 2006).

Spatial localization of the MR signal is achieved by the orthogonal application of short pulsed magnetic field gradients that superimpose on the main outer magnetic field B_0 enabling the possibility to locate the origin of the respective signal fractions that are induced in the receiver coil. Practically, three sets of electrical coils are integrated into the MR scanner system and produce weak magnetic fields that vary linearly along the x, y and z direction. The section selective z-gradient localizes the slice to be imaged while frequency and phase encoding gradients provide the segment of the slice along the x- and y-axis. The gradients alter the precession frequencies of protons. When the gradient fields are turned off, protons return to precession at their initial frequency but with a remaining permanent phase shift to protons outside the selected segment enabling the computation of the exact location and amplitude of the signal (Bitar et al. 2006; Dale et al. 2015).

In order to create a set of images with different contrasts and highlighted tissue a programmed set of changing gradients and RF pulses is tailored into different sequences

that are grouped in the MR protocol. The raw MR signal data is sampled and stored in k-space during the measurement, a matrix of voxels representing the spatial frequency information. The trajectory of k-space sampling can be for example cartesian, radial or spiral with varying density. The observed MR signals from a scan typically contain over 4 million small voxels specifying all three-dimensional resolution units of the probed subject. During final data reconstruction the raw signal data set is mathematically processed by a discrete inverse or more sophisticated Fourier Transformation to produce the final MR image.

1.3 Quantitative Magnetic Resonance imaging

Although qualitative parameter mapping is still the gold standard for MRI examinations in the clinical setting, the method comprises disadvantages. Conventional parameter weighted images allow to distinguish between severe morphological abnormalities which display a signal contrast between pathological and non-pathological tissue. Tissue is referred to as being hyperintense or hypointense compared to another structure. Hence, while relative comparisons are possible, there is a lack of assessment of absolute property values, limiting objective and standardized comparisons of structural differences of tissues. Moreover, subtle or smallest pathologic changes such as dysplastic tissue transition indicating malicious transformation may not be recognized (Ma et al. 2013). Structural variations found for example in tumorous edema, necrotic tissue, demyelination or axonal loss may lead to similar or even no significant image contrast and therefore limit diagnostics of qualitative MRI (Pierpaoli 2010). Because of the weighted-image character, conventional MRI is also insensitive to global parameter- or structural changes that might affect larger tissue compartments.

In the past decade, much effort has been invested in the development of rapid quantitative MR approaches. First mapping techniques to quantify T_1 and T_2 relaxation times were based on single parametric methods requiring several acquisitions wherein one specific acquisition parameter varied while others were kept constant (Look and Locker 1970; Huang et al. 2007). T_1 measurements involved either free induction decay of saturation or inversion recovery spin echo methods (IR-SE) (Carr and Purcell 1954; Crawley and Henkelman 1988; Deoni et al. 2003) while T_2 measurements were based on spin echo sequences such as the Carr-Purcell-Meiboom-Gill sequence (CPMG) (Meiboom and Gill 1958; Hahn 1950; Deoni 2010). Several images were generated in a row from repetitive acquisition patterns each with a different inversion time for T_1 or echo time for T_2, keeping other acquisition parameters constant. From the multiple values of each voxel an exponential curve was modeled with T_1 and T_2 relaxation times as decay. However, one major drawback of such

single-parametric methods lies in the reduced time efficiency. Hence, multi-parametric mapping techniques have been proposed to quantify multiple imaging parameters simultaneously to overcome long scan times. These methods use sequences from which the signal displays a combined function of multiple imaging parameters. T_1 and T_2 can be obtained simultaneously at each point of the recovery curve by fitting one signal model (Warntjes et al. 2008; Warntjes et al. 2007).

While scan time was considerably decreased by the invention of multi-parametric methods, major challenges concerning the repeatability and accuracy of common quantitative MRI techniques remain and limit a potential application in the clinical setting (Ma et al. 2013).

1.4 Magnetic Resonance Fingerprinting

Introduced in 2013 by Ma et al. at the Case Western Reserve University (Cleveland, Ohio, USA), MRF emerged as a robust mapping technique with an acquisition time comparable to common qualitative MR protocols. Taking a whole new approach to quantitative mapping, various tissue parameters are simultaneously examined in a single acquisition (Ma et al. 2013). The MRF technique consists of an innovative data acquisition, post processing and visualization method. A sketch of the MRF framework is presented in figure 1. During a single scan, acquisition parameters are varied in a pseudorandom manner triggering each tissue to generate a unique signal evolution. A database, called the dictionary contains pre-computed physiologically possible signal evolutions from realistic tissue parameter combinations. These signal vectors, simulations of MR related identification features like T_1 and T_2 relaxation times, relative spin density, diffusion or B_0, are generated on the basis of the Bloch equation formalism (Bloch 1946; Doneva et al. 2010). Once the data acquisition is completed, a pattern recognition algorithm is used to match the dictionary entry that represents the acquired signal evolution best for each voxel. Subsequently, the parameters from the simulated signal vector are ascribed to this voxel (Coppo et al. 2016). These directly measured tissue features enable quantitative examinations of tissue-specific properties to provide information that can improve diagnostics, prognosis and therapeutic options of various diseases. Thus, MRF seems to be highly promising for the application in daily clinical MR imaging workflows. This section gives a brief overview of the framework and fundamental elements of the MRF method/implementation.

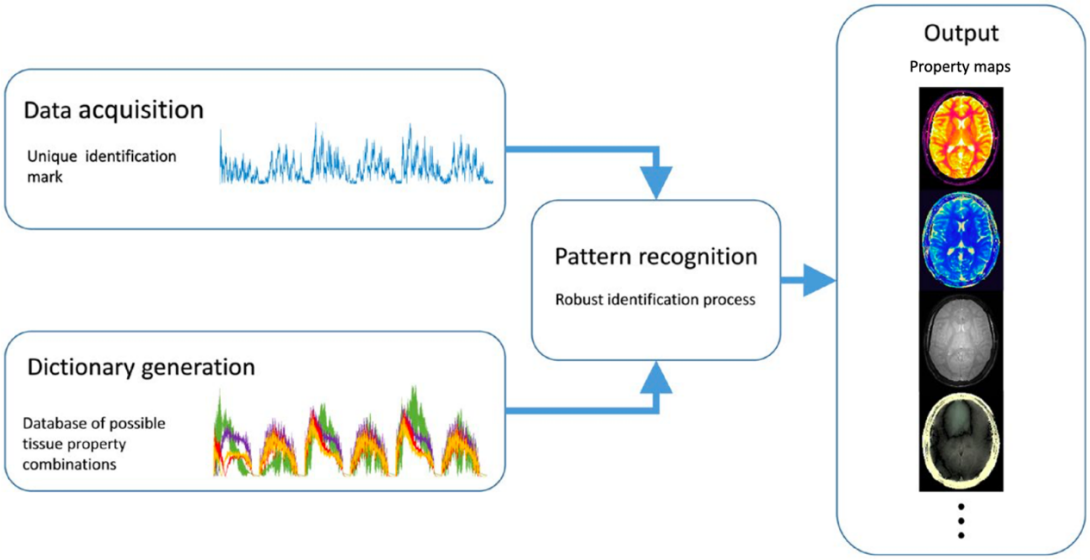

Figure 1 (original scheme, taken from (Mehta et al. 2019), permission granted by John Wiley & Sons): Left: Unique signal evolutions from pseudorandom acquisition parameters are characteristic of tissue types. The dictionary contains precomputed simulated tissue responses. A pattern recognition algorithm identifies the dictionary entry matching the acquired signal. Right: From the identified database entry, tissue characteristics are assigned to each voxel to generate sets of property maps.

1.4.1 Data acquisition, 'the fingerprint'

Standard quantitative mapping techniques require several acquisitions wherein the acquisition pattern of the flip angle (FA), repetition time and the phase of radiofrequency pulses repeats constantly in a particular sequence until all data in k-space is obtained. Subsequently, images weighted by a particular property are constructed. In contrast to this, MRF recovers all parameters directly and simultaneously from a single pseudorandomized acquisition. During this acquisition, parameters such as the FA, the phase of the RF pulse, TE and TR are continuously varied in a pseudorandom manner.

The initial implementation of MRF was based on an inversion-recovery-prepared balanced steady state free precession sequence (bSSFP) which is particularly sensitive to T_1 and T_2 relaxation times and has already been extensively studied for spin behavior (Schmitt et al. 2004). Figure 2 displays an overview of the MRF acquisition framework with two different acquisition patterns. Figure 2a shows the sequence diagram with formation of RF excitation pulses, slice selection gradients and readout. For k-space sampling one variable density spiral trajectory was used per repetition time (minimum-time gradient design, figure 2b (Hargreaves et al. 2004)). Two sequence patterns used for the first implementation of MRF are shown in diagrams 2c and d. A noise-function called Perlin noise, based on pseudorandom gradient vectors was used to generate a series of flip angels (Ma et al. 2013). This FA pattern was combined with a random repetition time from a uniform random

number generator (figure 2c). The second flip angle pattern was composed of repeating sinusoidal curves with a period of 250 repetition times and alternating amplitudes (figure 2d). This variation was paired with a Perlin noise pattern of the repetition time. The variation fashion of FA and TR is only one example of a variety of possible acquisition patterns used in MRF. The implementation is not restricted to any specific set of parameters (Ma et al. 2016).

Over time, other sequences were implemented in MRF in order to overcome different disadvantages and limitations. Balanced SSFP for example may be affected by banding artifacts as a result from signal modulation due to B_0 field inhomogeneities. To overcome this artifact, the well-known Fast Imaging with Steady State Precession (FISP) sequence was adapted to MRF by Jiang et al. (Jiang et al. 2015). This sequence enables the quantification of relaxation parameters by retaining signal coherence by a constant unbalanced gradient moment in repetition time without bandlike signal loss from areas of increased B_0 inhomogeneity.

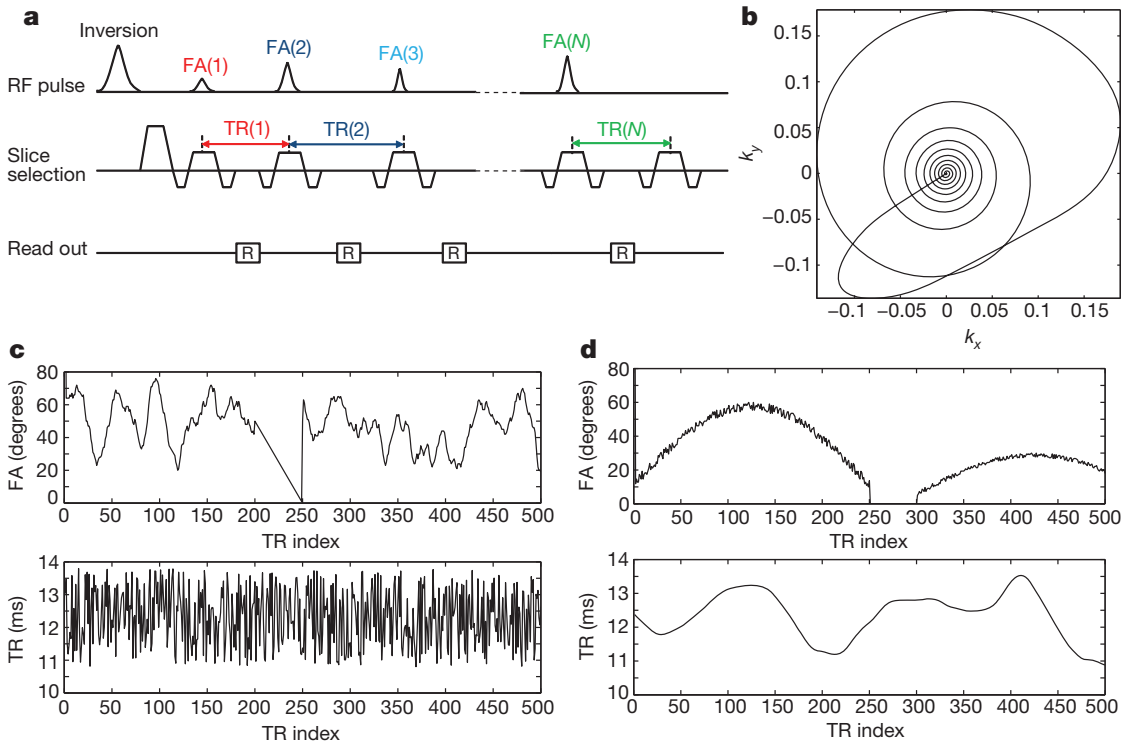

Figure 2 (original scheme, taken from (Ma et al. 2013), permission granted by Springer Nature): Overview of the initial MRF acquisition framework using the balanced steady state free precession sequence. Scheme a depicts the sequence diagram with formation of RF excitation pulses, slice selection gradients and readout. Plot b: Variable-density k-space sampling. Plot c: Pseudorandomized variation of flip angle composed of Perlin noise and a random repetition time ranging from 10.5 to 14 ms. Plot d: Repetitive sinusoidal variation of flip angle with a period of 250 acquisitions and alternating amplitudes. Perlin noise pattern for repetition time variation.

1.4.2 Dictionary generation

The acquired MRF signal or “fingerprint” needs to be matched to its unique counterpart from a database/collection of simulated fingerprints. The MRF dictionary therefore contains pre-computed signal vectors of all physiologically possible signal evolutions from realistic combinations of material and tissue parameters featuring T_1, T_2, relative spin density, B_0 or diffusion. The dictionary can be represented as a matrix with columns as simulated signal evolutions and rows as time points or TRs used in the MRF sequence. This entire collection of dictionary entries covers all observable profiles of MR signals acquired throughout the scan. This simulation of physical spin behavior/effects and signal evolution is realized using numerical computing programs and compression algorithms.

In the initial MRF framework by Ma et al. the Bloch equation formalism of MR was used to pre-compute magnetization dynamics as solutions of the Bloch equations (Doneva et al. 2010). For MRF methods utilizing fast imaging with steady state precession sequences the dictionary generation is based on the extended phase graph formalism (Weigel 2015; Jiang et al. 2015; Buonincontri and Sawiak 2016). Other sophisticated mathematical models for MRF dictionary generation have been studied for example for the quantification of vascular characteristics or the assessment of brain hemodynamics via MRF (Lemasson et al. 2016; Su et al. 2017). Regardless of the underlying computation model, the database entries are calculated for a comprehensive range of relevant combinations of relaxation parameters and tissue characteristics with variable resolution. According to typical physiological limits in brain tissue for example, herein T_1 usually ranges from 100 to 3000 ms, whereas T_2 typically ranges from 10 to 500 ms with a variable increment or resolution (Jiang et al. 2015; Badve et al. 2015).

The calculation of a complete MRF dictionary requires a few minutes on a desktop computer (Ma et al. 2013). But depending on the sequence design used and the tissue property values preferred, the number of dictionary entries easily grow up to millions. The dictionary resolution in turn affects the computation time of the MRF examination and the quality and accuracy of results. A finer resolution naturally provides more exact results at the expense of an increasing computation time (Ma 2015).

1.4.3 Pattern recognition

As the final and most distinctive step in the MRF framework, a pattern recognition algorithm matches the acquired voxel signal evolution i. e. “fingerprint” with the closest dictionary entry linked to a specific set of tissue properties. This identification of the corresponding

entry is realized by calculating the vector dot product between the acquired fingerprint and all dictionary entries. The dictionary entry corresponding to the maximum value of the dot product is chosen to represent the true signal evolution of a material. All corresponding tissue parameters previously used to generate the signal in the specific dictionary entry are then assigned to the voxel and therefore assessed simultaneously.

This rather simple inner product pattern matching process has shown to be time efficient, robust to artifacts due to undersampling and insensitive to motion artifacts. Both extreme k-space undersampling and motion errors due to subject movement lead to errors and deficient signal evolutions which are incoherent and uncorrelated with the predicted signals from the dictionary, thus being ruled out by the pattern matching algorithm (Ma et al. 2013; Jiang et al. 2015; Yu et al. 2018).

In order to extract quantitative maps of tissue parameters such as T_1 and T_2, pattern matching and visualization takes a few minutes on standard computers. Nevertheless, the more tissue parameters are favored the computing time for pattern matching will increase with the size of the dictionary. Therefore, efforts have been devoted to fasten the pattern recognition and matching process using a compressed dictionary or fast group matching algorithms to enable reconstruction accuracy to clinically relevant time scales (McGivney et al. 2014; Cauley et al. 2015).

1.5 Aim of this work

Absolute quantification of tissue properties bears the potential to enable reproducibility and comparability of MR imaging procedures in order to improve diagnosis and therapeutic assessment.

Magnetic resonance fingerprinting is efficient in the direct quantification of tissue-characteristic quantities such as T_1 and T_2 relaxation times. The method was introduced as a novel approach to fast quantitative magnetic resonance imaging that allows simultaneous measurement of multiple tissue properties during one single, rapid acquisition.

However, to establish quantitative imaging parameters such as relaxometry values in productive clinical usage, the measured T_1 and T_2 values must be stable and repeatable which means that variation in the data measured from different tissues can be reliably attributed to physiological differences rather than arising from hardware or methodological errors.

The work in hand therefore aims on the assessment of the stability and repeatability of MRF-derived relaxometry data in an imaging phantom, various non-pathologic brain tissues in

volunteers and a large patient cohort to gain insight into the overall transferability of MRF from phantom scans to human tissue and to investigate the options to integrate MRF into routine clinical workflows.

The main objectives of this work are:

1. Validation of the MRF method and implementation by evaluating the repeatability of T_1 and T_2 relaxometry estimates in repetitive scans of a standardized imaging phantom and determination of minimal data variability.
2. Description of the normal range of MRF-derived T_1 and T_2 relaxometry data in non-pathologic brain tissue in a healthy volunteer cohort and comparison of the inter-individual data variability to the phantom scan results in order to range the repeatability/accuracy of relaxometry measurements in human brain under well-controlled conditions.
3. Investigating the feasibility of MRF brain scans in the clinical environment and evaluating the long-term stability of the relaxometry measurements in human brain.

2. Material and Methods

This section provides a comprehensive overview of the study design, study subjects enrolled, measurement procedures and statistical analysis used to analyze resulting data in this work.

2.1 ISMRM System Phantom

Artificial imaging objects of known dimensions and parameters have been developed to evaluate and analyze the performance of various imaging instruments, thus providing a standardization of scanner systems essential to calibrate MRI machines and to compare implementations from different vendors and facilities (Keenan et al. 2018). Especially quantitative measurements of imaging parameters require standardization of MRI protocols and sensitive calibration objects to validate the accuracy of in vivo measurements. A stable and well-defined imaging phantom offers the opportunity to ensure that the repeatability and reproducibility of quantitative measurements is comparable over time, between subjects and different sites or imaging platforms. Therefore, this system phantom should allow for determination of basic imaging parameters characterizing properties of relevant physiological tissues such as relaxation times or proton density.

To date, various application-specific phantoms were introduced by different organizations including objects for structural brain, breast and dynamic cardiac measurements and many specific MR-based biomarkers such as diffusion or proton-density fat fraction (Keenan, Wilmes, et al. 2016; Keenan et al. 2018).

A prototype ISMRM/NIST system phantom to mimic brain scans used in this work, is shown in figure 3.

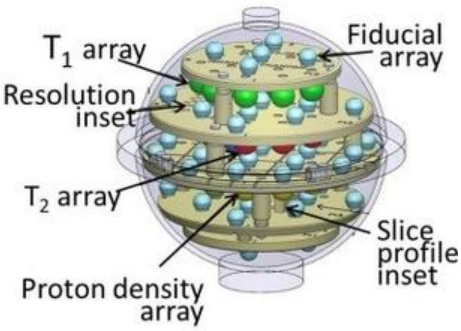

Figure 3: Scheme of the ISMRM/NIST system phantom used for repeated stability MRF scans. Horizontal PPS plate arrangement with integrated T_1, T_2 and proton density array composition inside (Image credit: NIST, 2021, via https://www.nist.gov/programs-projects/quantitative-mri).

It was recently introduced by the collaboration between the ISMRM Ad Hoc Committee on Standards for Quantitative Magnetic Resonance and the National Institute of Standardization and Technology (NIST 2016). A plastic sphere sizing a person's head

consists of a water-filled spherical polycarbonate shell with an inner diameter of 200 mm that fits standard MR head coils. The shell incorporates five polyphenylene sulfide (PPS) plates in coronal plane which are connected to PPS rods. Small sub-spheres of 1 cm diameter are arranged on the PPS plates forming a three-dimensional array framework (see figure 3). It is subdivided into a 14 element T_1 array, a 14 element T_2 array, a 14 element proton density array and several fiducial spheres distributed on the PPS spheres. The contrast spheres contain deionized/distilled water doped with solutions of different $NiCl_2$ concentrations. Analogous to human brain tissue parameters, the solution gets magnetized when subjected to a magnetic field. The composition of the sphere fill solutions is chosen in a way that relaxometry values cover large parameter ranges corresponding to typical relaxation times in human brain.

Within one day, repetitive MRF measurements of the phantom T_1 and T_2 relaxation times were performed consecutively in both a 1.5 T MRI system (MAGNETOM Aera, Siemens Healthineers, Erlangen, Germany) and a 3 T system (MAGNETOM Skyra, Siemens Healthineers, Erlangen, Germany) at the department of Radiology in the University Hospital Essen, Germany. The results were compared to reference values obtained on NMR by inversion recovery measurements (Keenan et al. 2018). Prior to every single scan, the phantom was positioned, adjusted and kept at rest for at least 30 minutes to prevent motion artifacts from solution fluctuations.

2.2 Study population

After approval of the local ethics committee, informed written consent was obtained from all patients and participants of the volunteer study. Both volunteer and patient collectives were scanned in the same scanner systems that were utilized for the phantom measurements before. All volunteer and patient measurements were performed at the department of Radiology in the University Hospital Essen, Germany.

2.2.1 Healthy volunteers

A total of 10 healthy volunteers with a mean age of 31.3 ± 3.2 years (age range 27 – 37 years, 4 male, 6 female) were enrolled in a preliminary study protocol during two consecutive measurement days. None of the subjects had a history of neurological pathologies, structural brain- or psychological diseases. Contrast-agent-free MRF brain scans with a total measurement time of 10 minutes per scan were performed on every volunteer subsequently three times in a row in both a 1.5 and 3 T MRI scanner system

(MAGNETOM Aera and Skyra, Siemens Healthineers, Erlangen, Germany). Obtained T_1 and T_2 values were averaged over these 3 scans for each volunteer. Prior to each actual MRF acquisition block, a transversal T_2 sequence was included in the scan routine for localization of the MRF slices.

2.2.2 Patients

After analysis and evaluation of the volunteer MRF data, MRF scans of patients at the department of Radiology in the University hospital Essen, were launched. In a time period of 6 months, a total of 92 patients with either various previously diagnosed neurological pathologies or suspected diagnosis of brain pathologies that were scheduled for a routine clinical protocol at 3 T received an additional MRF protocol. Patients with an age range of 21 to 80 years (mean age of 51.8 ± 14.8 years, 55 female, 37 male) were included in the cohort. The age distribution of the entire cohort can be extracted from table 1.

Age	21-30	31-40	41-50	51-60	61-70	71-80
n	13	9	15	28	17	10

Table 1: Age distribution in the patient cohort.

All patients underwent a conventional MRI examination within the scope of clinical diagnosis, therapy or staging management. After the regular MRI sequence block, every patient was additionally scanned using the MRF protocol in a 3 T MRI system (MAGNETOM Skyra, Siemens Healthineers, Erlangen, Germany) within the same scan session. All contrast-agent-free MRF brain scans were performed under the same experimental conditions and with the same sequence series used in the phantom and volunteer study before. The spectrum of diseases in the patient collective ranged from solid tumors including glioblastoma, meningioma, pituitary adenoma or brain metastases to infectious, vascular and demyelinating diseases like multiple sclerosis. A total of 26 subjects in the patient cohort did not show any brain pathology. This sub-group of the patient collective will be denoted as healthy patients in the following.

2.3 MRF implementation and acquisition parameters

The work-in-progress MRF software package used for all measurements reported in this work is part of a collaboration of Case Western Reserve University and University Hospital Essen with Siemens Healthineers (Erlangen, Germany). The non-commercial MRF sequence prototype based on a FISP (fast imaging with steady-state precession)

acquisition was implemented on the 1.5 and 3 T scanner system at the Department of Radiology of the University Hospital Essen. An automated B_1-correction was additionally integrated in the work-in-progress sequence to compensate bias from variations in the RF field- and main magnetic field strength. For the detection of MR signals a standard vendor provided 20-channel head RF receiver coil was used. The parameters of the pseudorandomized acquisition scheme were chosen as follows: The matrix size of 256 x 256 pixels covered a fixed field of view of 300 × 300 mm^2. The slice thickness was set to 5 mm. The flip angle varied from 0 to 60 degrees. The TR was 12 ms. The initial inversion recovery pulse enhancing T_1 differences between tissues was a sinc pulse with 800 µs duration and time-bandwidth product of 2. In a total acquisition time of 30.8 s, 3000 measurements were acquired for each slice.

In total, T_1 and T_2 maps were acquired from 3 two-dimensional reference slices covering the upper cranium, mid ventricular and cerebellar level for both study groups, the volunteer and the patient cohort. The slices were always set to the same position in both study groups independent of any pathologies. The overall examination time per study subject did not exceed 10 minutes. The acquisition of T_1 and T_2 MRF color maps was implemented in the image reconstruction routine of each scanner system.

2.4 Region of interest analysis

The obtained quantitative MRF T_1 and T_2 values were encoded in two-dimensional parameter maps. Their mean values were determined by defined regions of interest (ROI) which were evaluated using the image processing software OsiriX (open-source software; www.osirixviewer.com). In total, 14 circular ROIs were analyzed from the T_1 and T_2 arrays of the ISMRM phantom. For every volunteer / patient ROIs were manually drawn in the center of different anatomic regions including white and gray matter, basal nuclei, thalamus and cerebellar structures for the left and right hemisphere and central structures like genu and splenium of the corpus callosum and the mesencephalon. The ROI sizes usually ranging up to a few square millimeters depended on the actual size of the outlined anatomical structure. When placing the ROIs in the center of the sampled tissue, attention was drawn to the separation from neighboring structures in order to avoid partial volume effects. The total number of ROIs was 28 per healthy volunteer brain maps and included the following structures 12 bihemispheric structures: Superior frontal white matter, centrum semiovale, frontal white matter, nucleus caudatus, putamen, globus pallidus, thalamus, internal capsule, parietal white matter, frontal gray matter, temporal gray matter and the cerebellar lobe. 4 mid central structures of the mesencephalon, vermis and corpus callosum

genu and corpus callosum splenium were added. Regarding the patient cohort, particular structures notably suffering from imaging artifacts such as the partial volume effect for example were omitted in order to guarantee a fluent and reliable quantitative evaluation and analysis routine. Therefore, a total of 15 ROIs were analyzed from each patient brain map: 6 structures per hemisphere including the frontal white matter, nucleus caudatus, putamen, thalamus, parietal white matter, and the cerebellum and 3 tissues of the corpus callosum genu, corpus callosum splenium, and mesencephalon in mid central positions. Since this work focuses on the quantification of relaxometry data from healthy brain tissue, only non-pathological tissues of the mentioned anatomic regions of the upper, middle and lower level were included into the ROI analysis. If structures with diseased tissue or obvious artifacts were discovered in the prescribed anatomic segments to analyze, these structures were skipped and excluded from the data collection.

2.5 Statistical analysis

The extracted quantitative T_1 and T_2 data were subsequently saved into a relational database managed by SQL (structured query language) for further analysis and selection of different data subgroups. Raw relaxation data is given by mean values plus averaged standard deviation of a ROI segmented region for every study subject. Graphic and statistical data analysis has been performed on the scientific graphing and data analysis software Origin (Origin 2020 for Windows 10). Box-and-whisker plots were used to visualize the variance of the T_1 and T_2 data sets from the volunteer and patient cohort. The box plots are generated such that the upper and lower edge of each box indicates the first and third data quartile respectively. The inner-box line represents the second quartile or median and the small in-box square is the mean T_1 or T_2 value. The whiskers extend from the top of the box to the maximum data value that is $\leq$ 1.5 times the interquartile range and down from the bottom of the box to the minimum data value that is $>$ 1.5 the interquartile range. All values outside this area are considered as outliers.

The repeatability and variability of MRF-derived relaxometry estimates in the phantom and both healthy volunteer and patient group is characterized by the coefficients of variation ν_{T1} and ν_{T2} which are defined as the ratio of the standard deviation to the mean T_1 and T_2 values. In case of the phantom measurements, the mean T_1 and T_2 values are calculated over 6 successive MRF scans. Concerning the volunteer and patient measurements, the T_1 and T_2 correlation coefficients are calculated from the mean T_1 and T_2 values of all subjects of the corresponding cohort.

Linear regression analysis was used for the comparison of phantom data from MRF and NMR methods in chapter 3.1. The correlation strength between the T_1 and T_2 values derived from MRF and NMR methods was evaluated by Pearson's correlation coefficient R^2. The coefficient provides values between 0 and 1, indicating a strong (linear) correlation of two variables for R^2 values close to 1. Bland-Altman plots were added to quantify the agreement between both methods. The bias and 95%-limits of agreement of the plots represent the mean difference and the range of variation between the relaxometry values obtained from MRF and NMR techniques, respectively.

A linear regression model was also used to assess the relationship between age and relaxometry in the patient cohort. Hereby, a p-value < 0.05 was considered significant.

3. Results

3.1 Phantom study

In an initial MRF measurement series relaxation time measurements from 6 phantom scans were performed each at 1.5 and 3 T. The T_1 and T_2 relaxation times were analyzed with respect to their variability throughout different successive scans in order to test the stability and repeatability of the MRF implementation. The obtained quantitative relaxometry values encoded in two-dimensional parameter maps are exemplarily shown in figure 4.

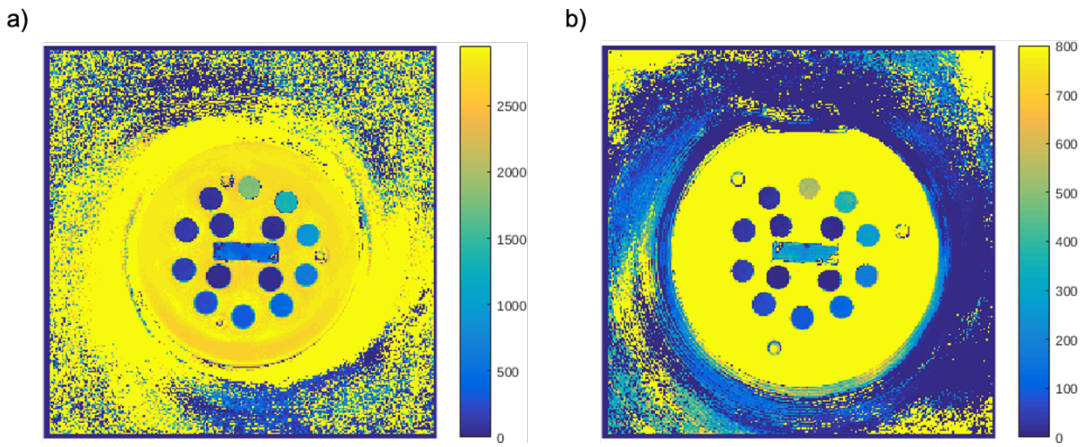

Figure 4: T_1 (a) and T_2 (b) maps obtained from MRF scans of the ISMRM system phantom arrays at 3 T.

Figure 5 presents the T_1 (fig. 5a and c) and T_2 (fig. 5b and d) measurements of each compartment 1 to 14 sorted by their position inside the phantom. The repeatability coefficients of variation of the T_1 and T_2 estimates calculated as the dispersion over 6 scans (= inter-scan variation) are shown in figure 6.

Regarding T_1 data, the inter-scan variability amounts to a maximum of 6.92 % (region 13) and minimum of 0.27 % (region 9) at 3 T. At 1.5 T, the coefficient of variation of T_1 ranges between 6.56 % (region 12) and 0.74 % (region 8). Regarding T_2, higher variation for all regions is observed. At 3 T, the inter-scan variation lies between 13.67 % (region 11) as maximum and 0.75 % (region 7) minimum. At 1.5 T, the maximum is 13.9 % (region 12) and 1.76 % (region 13) is the minimum T_2 variation.

In general, all measurements show smaller variations of both longitudinal and transverse relaxation in the higher time ranges (regions 1-9) and higher coefficients of variation in the smaller time ranges (regions 10-14). Overall, the mean T_1 variation across all regions does not exceed 2.7 % at both field strengths. The mean variation of T_2 values amounts to 4.41 % at 1.5 T and 5.41 % at 3 T.

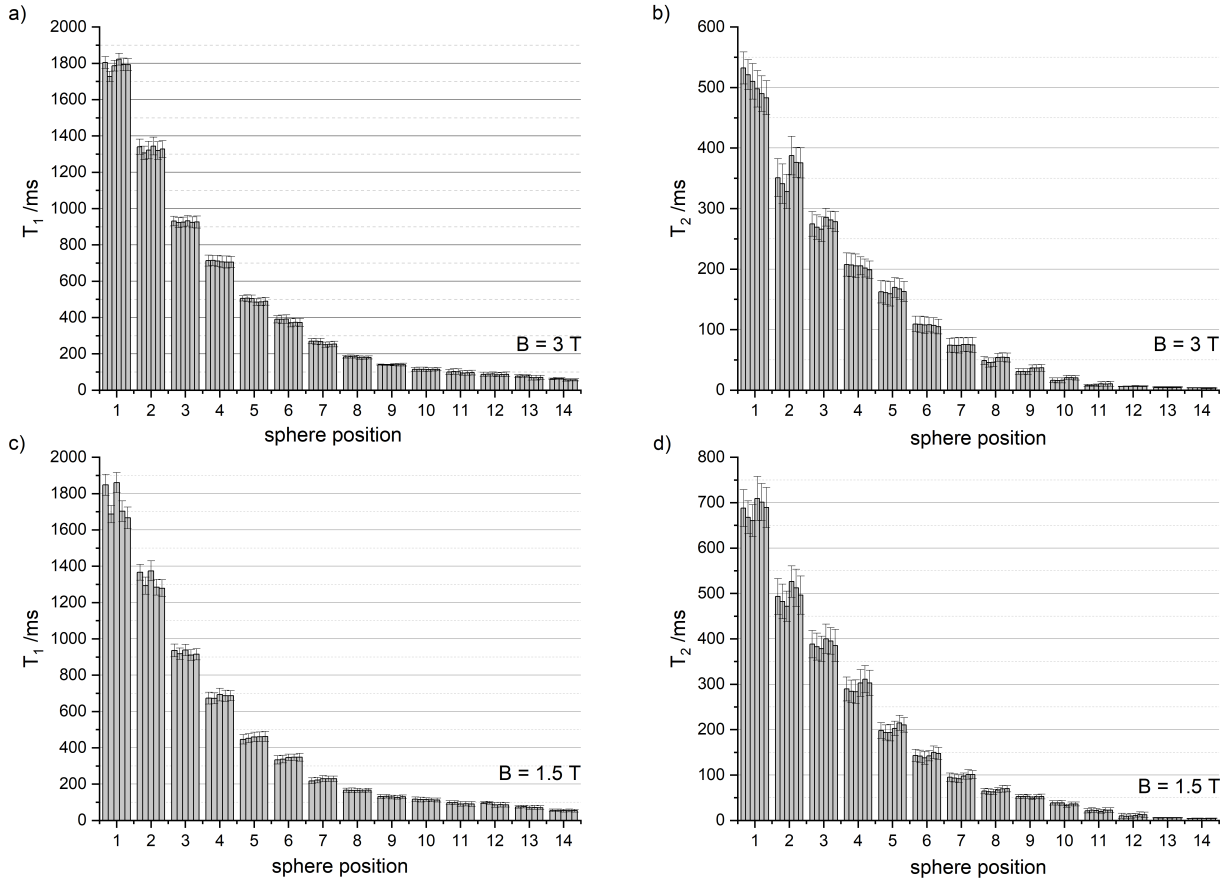

Figure 5: Relaxometry measurements in the ISMRM phantom: Upper plots show pooled bars of T_1 (plot a) and T_2 (plot b) values of each sphere of the phantom over 6 (5 in case of T_1 measurements at 1.5 T) successive MRF scans measured at 3 T. Lower plots show the T_1 (plot c) and T_2 (plot d) results of the same measurements at 1.5 T. Error bars indicate the inner-ROI standard deviation (Note that in case of scans at 1.5 T, the T_1 dataset contains only 5 repetitions because of local exceptional data loss during storage).

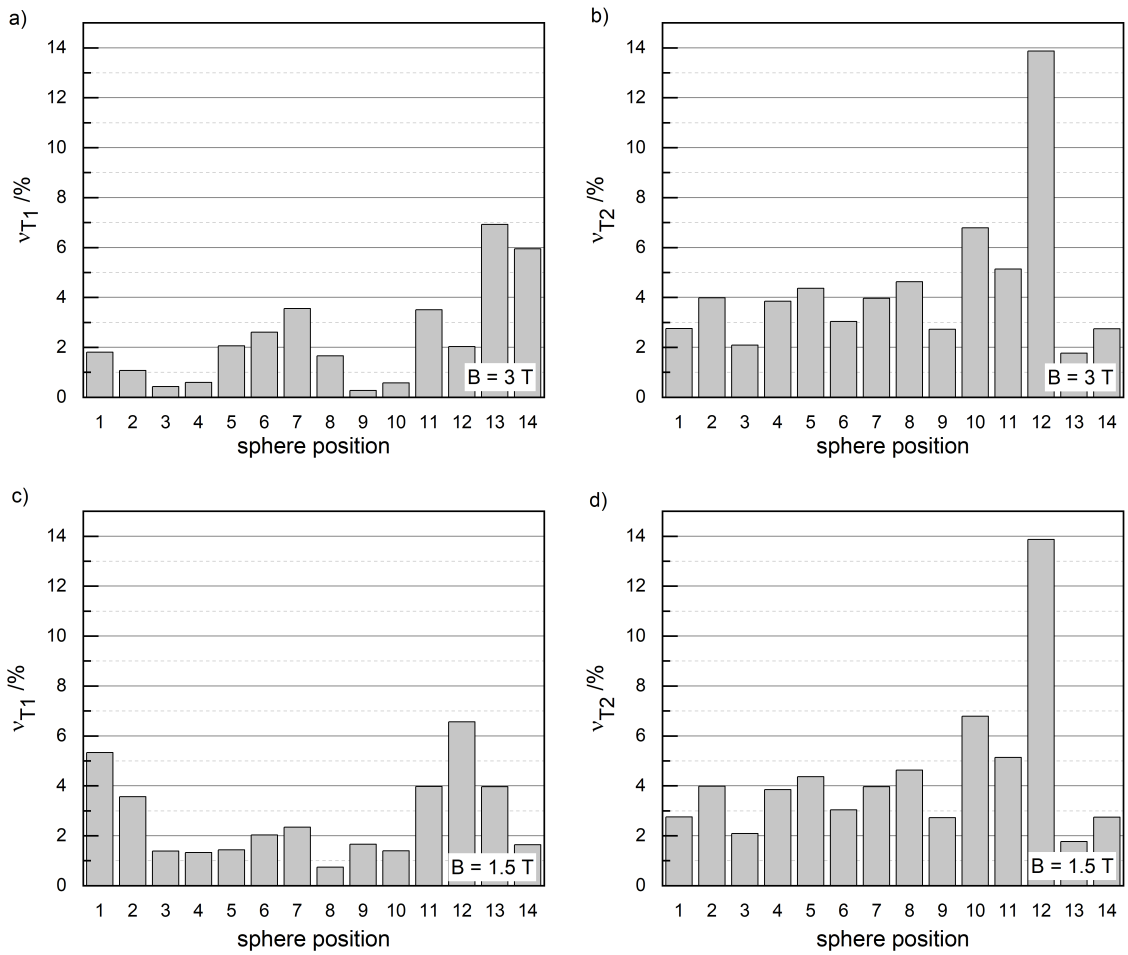

Figure 6: Repeatability of the T_1 (plot a and c) and T_2 (plot b and d) estimates from 6 (5 in case of T_1 measurement at 1.5 T) MRF phantom scans assessed by the coefficients of variation ν_{T1} /% and ν_{T2} /% at 3 and 1.5 T.

In order to assess the accuracy of the MRF results in the phantom, the MRF-derived T_1 and T_2 data were compared to their corresponding values obtained from gold standard quantitative NMR mapping techniques. The quantitative relaxation times from the ISMRM system phantom obtained by an inversion recovery spin echo sequence (IR-SE) for T_1 estimation and a multiple single-echo spin echo method (CPMG) for T_2 measurements were taken from a publication of Keenan et al. in 2016 (Keenan, Stupic, et al. 2016). Figure 7 and 8 present the MRF-derived T_1 and T_2 estimates generated from each sphere of a system phantom scan at 3 T (figure 7) and 1.5 T (figure 8) in comparison to the reference relaxometry values from spin echo methods described above by means of a correlation analysis and corresponding Bland-Altman plots.

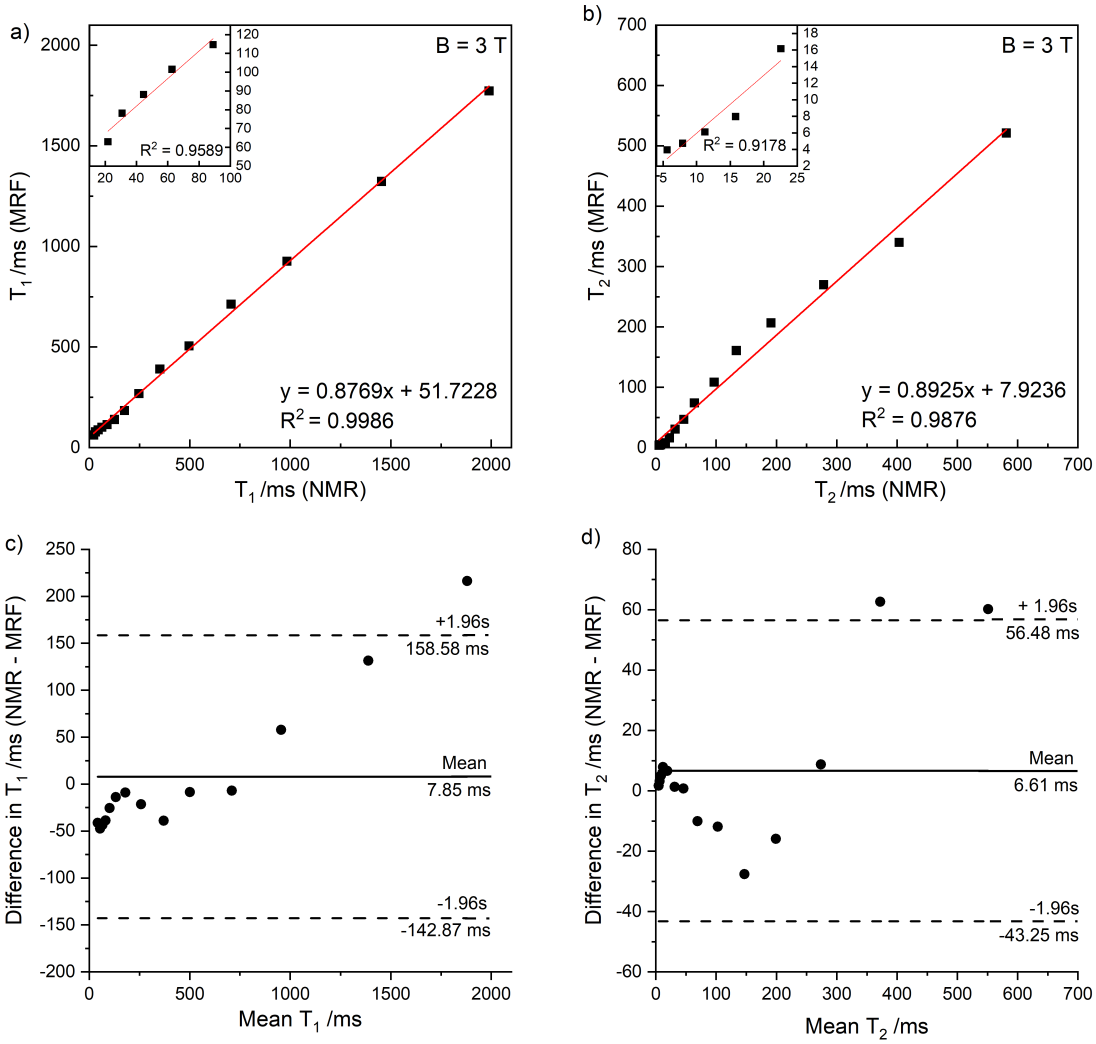

Figure 7: Correlation plots comparing the T_1 and T_2 values calculated from MRF scans with T_1 and T_2 values derived from NMR inversion recovery spin echo and spin echo methods at 3 T (plots a and b, NMR relaxometry data taken from (Keenan, Stupic, et al. 2016)). Red curves in fig. 7a and b present linear regressions of the data points in each plot. The insets show correlation plots of small T_1 and T_2 time ranges up to 120 and 16 ms respectively. Bland-Altman plots in figure 7c and d show the bias (solid line) as mean difference and 95%-limits of agreement interval (dashed lines, mean difference ± 1.96 times standard deviation) as the range of variation betweenT_1 and T_2 values from MRF scans with corresponding values obtained from NMR inversion recovery spin echo and spin echo methods at 3 T.

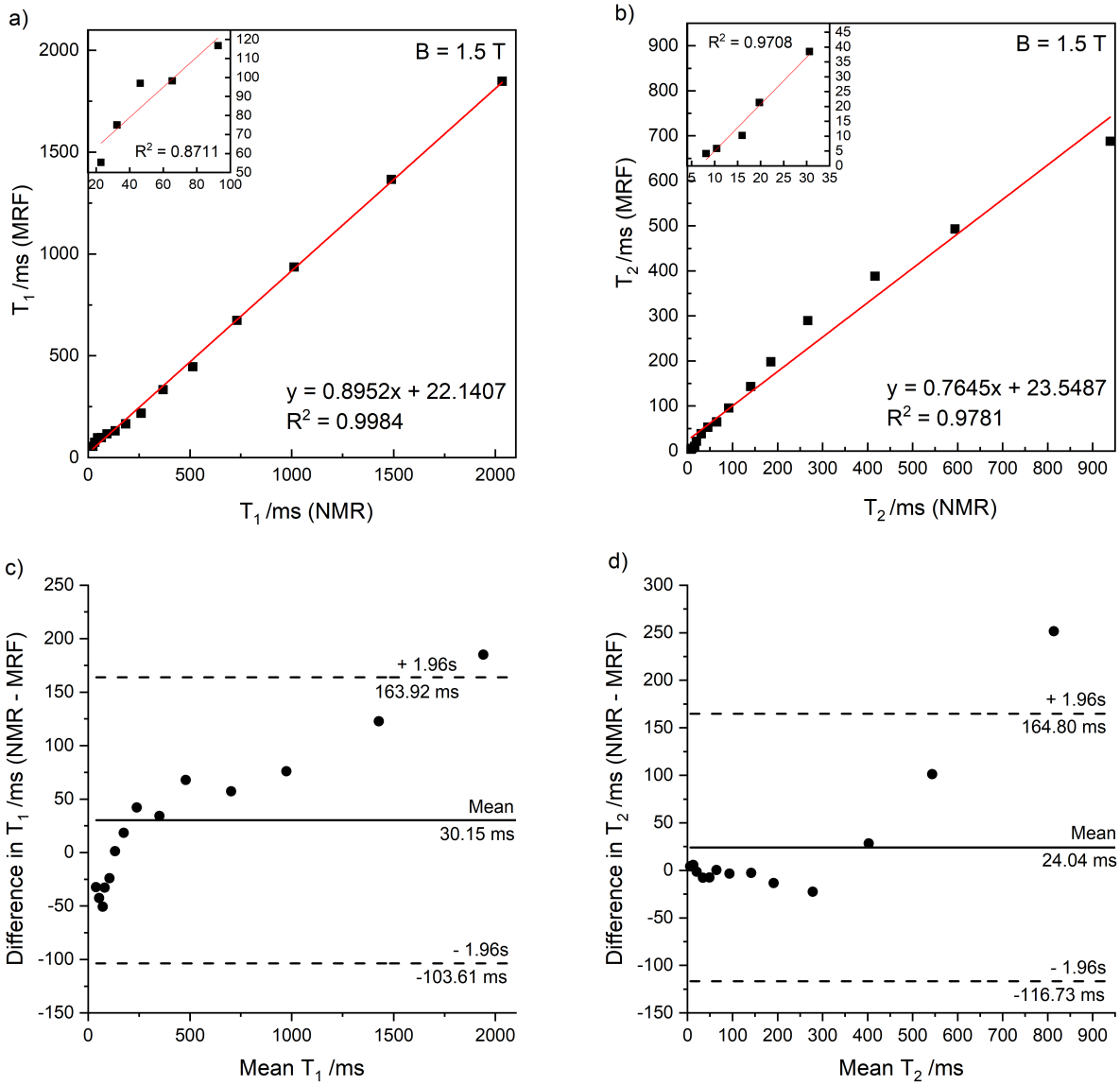

Figure 8: Correlation plots comparing the T_1 and T_2 values calculated from MRF scans with T_1 and T_2 values derived from NMR inversion recovery spin echo and spin echo methods at 1.5 T (plots a and b, NMR relaxometry data taken from (Keenan, Stupic, et al. 2016)). Red curves in fig. 8a and b present linear regressions of the data points in each plot. The insets show correlation plots of small T_1 and T_2 time ranges up to 120 and 40 ms respectively. Bland-Altman plots c and d show the bias (solid line) as mean difference and 95%-limits of agreement interval (dashed lines, mean difference ± 1.96 times standard deviation) as the range of variation betweenT_1 and T_2 values from MRF scans with corresponding values obtained from NMR inversion recovery spin echo and spin echo methods at 1.5 T.

Measurements at 3 T display T_1 values with a strong correlation of $R^2 = 0.9986$ to the results from Keenan et. al (fig. 7a). The T_2 results show a (non-linear) correlation to NMR data (fig. 7b). Bland Altman plots show relatively small differences in the T_1 and T_2 values between MRF and NMR values except for the longest relaxation times (both T_1 and T_2) which were outside of the 95%-limits of agreement.

Figure 8 displays corresponding correlation- and Bland-Altman plots for comparison and assessment of the agreement of relaxometry values of the MRF method and inversion recovery spin echo and spin echo methods at 1.5 T. Analogous to the results obtained at 3 T, the correlation of T_1 values between both measurement methods is strong with a coefficient of correlation of $R^2 = 0.9984$. A correlation is also given in case of T_2 values but it is again not linear as already demonstrated for T_2 results at 3 T. Bland Altman plots again suggest a good agreement between both methods. At both field strengths, the highest T_1 and T_2 values lie outside the limits of agreement.

With the maximal correlation coefficient of $R^2 = 0.9986$ (3 T) and $R^2 = 0.9986$ (1.5 T), the T_1 values show a very good correlation to the T_1 values obtained from gold standard quantitative NMR mapping techniques in the referred publication of Keenan et. al at both field strengths. The correlation of T_1 values is even stronger when only values in the upper time range from 170 to 2000 ms are included. Here, correlation coefficients are calculated as $R^2 = 0.9996$ at 1.5 T and $R^2 = 0.9991$ at 3 T. As shown in the insets of fig. 7a and fig. 8a the T_1 correlation is definitively poorer in time range smaller than 170 ms.

T_2 values in general tend to deviate more from their reference values. At both field strengths, a correlation of T_2 values between MRF and NMR data is given but does not seem to be linear. Similar to the T_1 data, the correlation of T_2 values between MRF and NMR data is poorer for small time ranges up to 30 ms (see insets of fig. 7b and fig. 8b) and improves for larger time ranges from 30 to 600 ms. Overall, at both field strengths, T_1 and T_2 values measured with MRF bear a consistent tendency to underestimate the long relaxation times and overestimate the short relaxation times. The time ranges where high correlation of the relaxometry estimates is obtained, cover physiological time ranges of T_1 and T_2 in human brain.

In general, all measured T_1 and T_2 values from the MRF method agreed well with the reference values as given by NIST. The phantom results from repetitive scans reveal the stability and repeatability of the MRF technique. The comparability of the results to the NMR gold standard method shows an acceptable accuracy of the MRF implementation, hence serving as a reference for the following in-vivo studies in the present work.

3.2 Healthy volunteer study

In this section, MRF derived relaxometry measurements are tested for inter-individual repeatability in a total of 10 healthy volunteers. All results were obtained in two consecutive days with 5 subjects scanned each day.

3.2.1 T_1 and T_2 quantification in different anatomic regions

Figure 9 shows the T_1 map derived from a MRF scan of one of the healthy volunteers visualizing different anatomic reference slices of the upper cranium, mid ventricular and cerebellar level with all positions of ROIs included in the analysis. The brain levels shown in this figure represent the reference slices scanned during the imaging procedure. A total of 28 ROIs (12 per each hemisphere and 4 in central positions in the mid ventricular and cerebellar level) containing a compilation of cerebral white and cortical gray matter sections and important structures of basal nuclei, the thalamus and cerebellum were manually segmented in the T_1 map and automatically copied to the T_2 map.

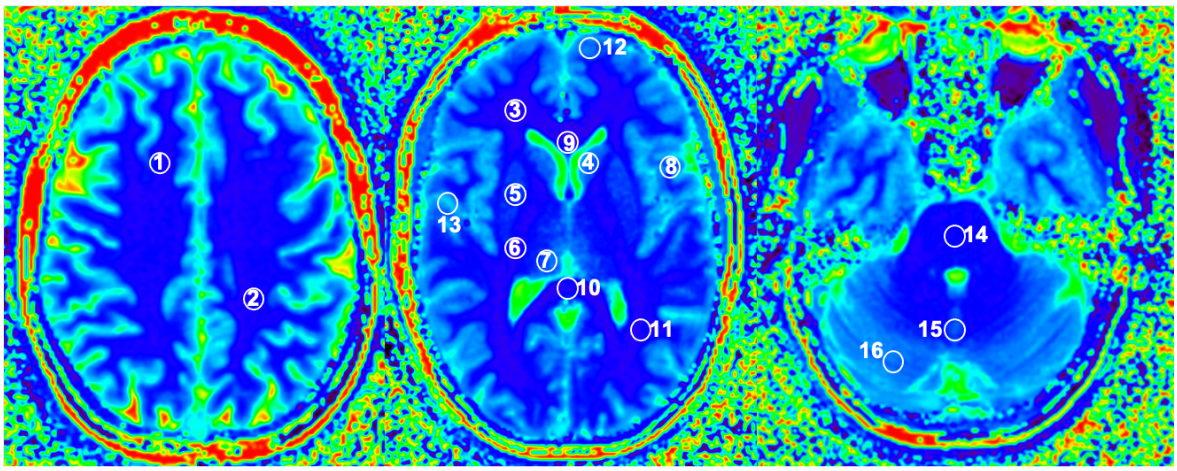

Figure 9: T_1 map with reference ROI placement for MRF measurements in healthy volunteers: 1: Superior frontal white matter, 2: Centrum semiovale, 3: Frontal white matter, 4: Nucleus caudatus, 5: Putamen, 6: Globus pallidus, 7: Thalamus, 8: Internal capsule, 9: Corpus callosum genu, 10: Corpus callosum splenium, 11: Parietal white matter, 12: Frontal gray matter, 13: Temporal gray matter, 14: Mesencephalon, 15: Vermis, 16: Cerebellar lobe.

For data analysis, relaxometry values derived from bihemispheric structures (white and gray matter, nucleus caudatus, putamen, globus pallidus, thalamus, internal capsule, cerebellar lobe) were averaged for every subject. Each subject was scanned 3 times in a row and mean relaxometry values were calculated as an average over these scans. Figure 10 shows the T_1 and T_2 values from 16 different anatomic brain regions obtained by MRF at 3 T (fig. 10a and b) and 1.5 T (fig. 10c and d) as box plots. The absolute mean T_1 relaxation times vary from around 900 to 1500 for a 3 T scanner and display a range from 680 to 1200 ms at 1.5 T. Small distributions of T_1 values represented by short boxes without outliers are found for white matter structures (superior frontal-, frontal- and parietal white matter and centrum semiovale) and for basal nuclei. Measurements of the frontal white matter for example, show ranging T_1 values from 823.117 ms to 907.588 ms at 3 T (fig. 10a) and from 618.907 ms to 690.073 ms at 1.5 T (fig. 10c). Wider distributions and scattered data are

found for the structures of corpus callosum genu and splenium, gray matter, vermis and cerebellum indicating a large inter-individual variation of the values at both 1.5 and 3 T. Regarding the cerebellum for example, T_1 values range from 1225.293 ms to 1440.359 ms at 3 T (fig. 10a) and from 961.839 ms to 1132.7 ms at 1.5 T (fig. 10c). Especially the T_1 data observed from corpus callosum genu and splenium and gray matter is skewed representing asymmetric data distribution in relaxometry values measured from these tissues.

For T_2 estimates, the mean values considering all anatomic regions range from around 30 to 73 ms in a 3 T scanner and from 40 to 70 ms at 1.5 T. Similar to the T_1 results, small boxes indicating low inter-individual variability are derived from white matter structures and basal nuclei. Oppositely to the T_1 data derived from these tissues the T_2 data display outliers beyond 1.5 times the interquartile range in some of these structures. For example, measurements of the frontal white matter show ranging T_2 values from 30.435 ms to 36.329 ms at 3 T (fig. 10b) and from 39.423 ms to 42.916 ms (with outliers at 34.021 ms and 46.12 ms) at 1.5 T (fig. 10d). Wider data dispersion and skewed boxes are found for T_2 values measured from the structures of corpus callosum genu and splenium, gray matter, vermis and cerebellum indicating a large inter-individual variation of the values at both fields similar to the results of the T_1 data sets. Regarding the cerebellum for example, T_2 values range from 49.004 ms to 67.912 ms at 3 T (fig. 10b) and from 58.13 ms to 77.618 ms at 1.5 T (fig. 10d).

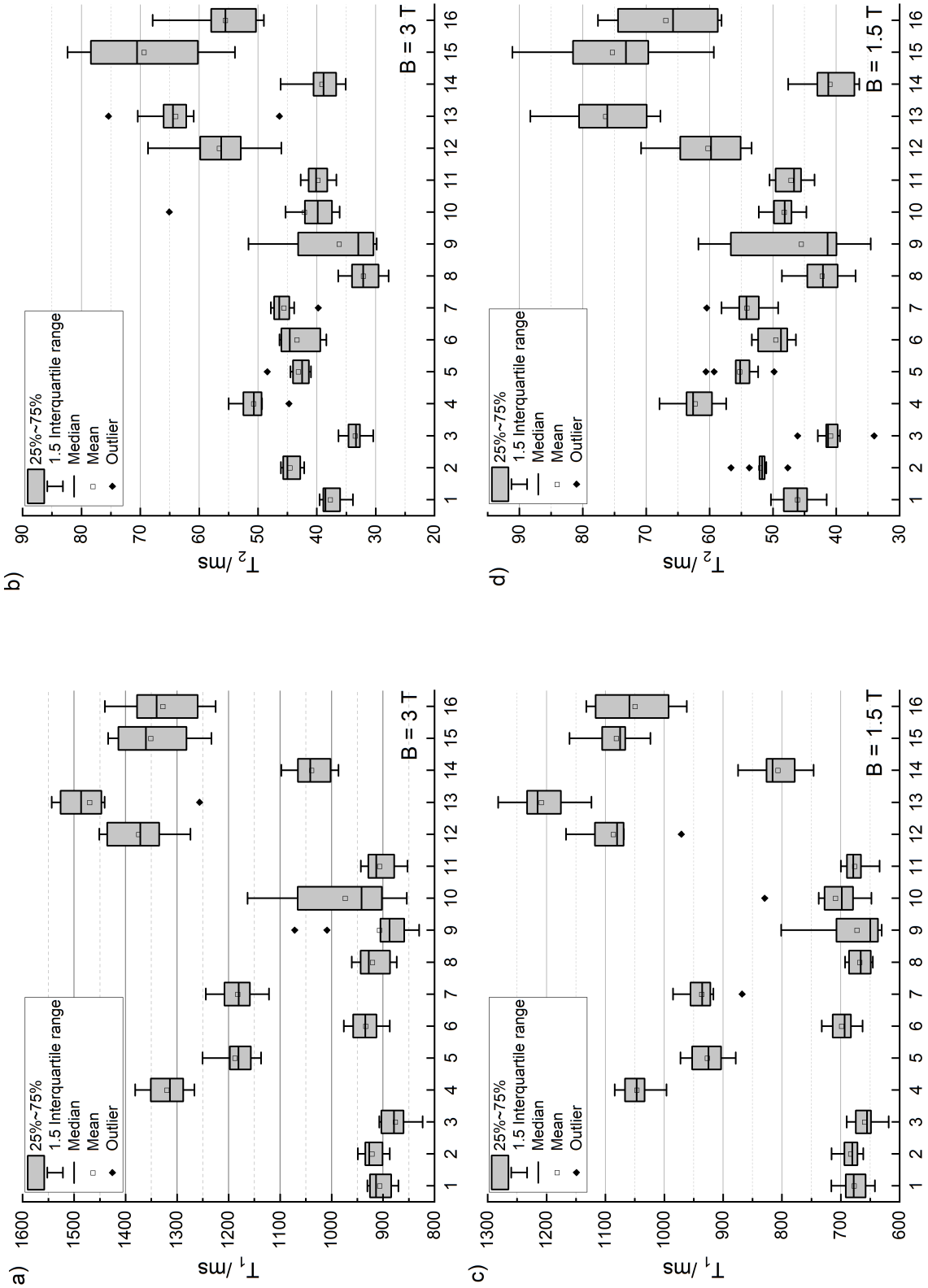

Figure 10: Box plots from T_1 and T_2 values from 16 different anatomic brain regions obtained by MRF at 3 T (plots a and b) and 1.5 T (plots c and d) in a total of 10 healthy volunteers. The upper and lower edge of each box indicates the first quartile and third quartile respectively. The inner-box line represents the median and the small square in the box is the mean. The whiskers extend from the top of the box to the maximum data value that is ≤ 1.5 times the interquartile range and down from the bottom of the box to the minimum data value that

is > 1.5 the interquartile range. All values outside this area are considered as outliers and represented as rhombs. X-axes: Anatomic regions: 1: Superior frontal white matter, 2: Centrum semiovale, 3: Frontal white matter, 4: Nucleus caudatus, 5: Putamen, 6: Globus pallidus, 7: Thalamus, 8: Internal capsule, 9: Corpus callosum genu, 10: Corpus callosum splenium, 11: Parietal white matter, 12: Frontal gray matter, 13: Temporal gray matter, 14: Mesencephalon, 15: Vermis, 16: Cerebellar lobe.

3.2.2 Analysis of data repeatability

The repeatability of relaxometry measurements was assessed by the coefficients of variation ν_{T1} and ν_{T2}. Figure 11 depicts the extent of the T_1 and T_2 variability ordered by all assessed anatomic regions.

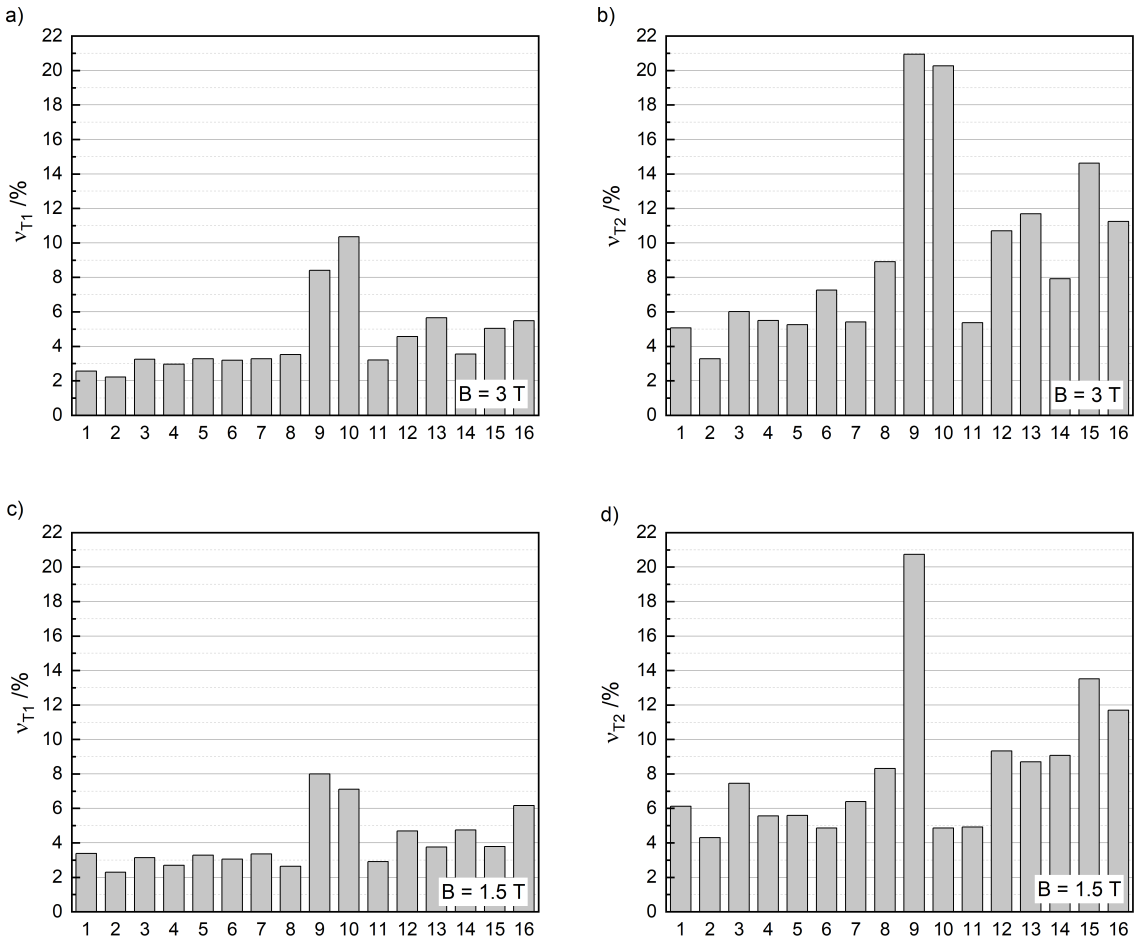

Figure 11: Repeatability of the T_1 (plot a and c) and T_2 (plot b and d) values from MRF measurements at 3 and 1.5 T ordered by 16 anatomic regions. ν is calculated as the ratio of the standard deviation to the mean T_1 and T_2 values from 10 healthy subjects. X-axes: Anatomic regions: 1: Superior frontal white matter, 2: Centrum semiovale, 3: Frontal white matter, 4: Nucleus caudatus, 5: Putamen, 6: Globus pallidus, 7: Thalamus, 8: Internal capsule, 9: Corpus callosum genu, 10: Corpus callosum splenium, 11: Parietal white matter, 12: Frontal gray matter, 13: Temporal gray matter, 14: Mesencephalon, 15: Vermis, 16: Cerebellar lobe.

Regarding T_1 values, the coefficient of variation is minimal in the white matter of the centrum semiovale at both field strengths (ν_{T1} = 2.44 % at 1.5 T, ν_{T1} = 2.37 % at 3 T). Minimal variation of T_2 values is also yielded from the area of centrum semiovale (ν_{T2} = 4.48 % at 1.5 T, ν_{T2} = 3.85 % at 3 T) at both 1.5 and 3 T. Additional low coefficients of variation of T_1 and T_2 are found for the tissues of all white matter, basal nuclei and the internal capsule at both field strengths. The largest coefficients of variation are obtained for the splenium and genu of corpus callosum (regions 9 and 10) for both T_1 and T_2 values independent of the field strength. For T_1, the maximum variation of ν_{T1} = 10.18 % is found in corpus callosum genu at 3 T. The variation of the T_2 values is maximum ν_{T2} = 21.62 % in corpus callosum genu measured at 1.5 T. Higher coefficients of variations are also deduced from gray matter tissue, the vermis and cerebellum for both T_1 and T_2 values (see fig. 11, regions 12, 13, 15, 16).

Omitting the results obtained from the corpus callosum genu and splenium, the coefficients of variation from both T_1 and T_2 found for all other anatomic regions are comparable to the corresponding variations measured from the ISMRM phantom, thus confirming the measurement stability and repeatability of characteristic MRF relaxation times in healthy brain tissue.

3.3 Patient study

After phantom validation and description of the normal range of MRF-derived relaxometry values in the volunteer cohort, patient scans were launched in order to investigate the integration of the MRF method into routine clinical workflows. The mean T_1 and T_2 values from different anatomic regions in a total of 92 patients were evaluated regarding their repeatability and comparability to the previous results from the volunteer cohort presented in section 3.2. All patient scans were performed on a 3 T scanner. The dependence of the relaxometry data on different age ranges will be presented in section 3.3.2.

3.3.1 T_1 and T_2 quantification and repeatability

In the following, a comparison of the relaxometry data at 3 T from a total of 92 patients with the results provided by the healthy volunteer cohort is presented. For the analysis 9 anatomic regions in the cerebrum, cerebellum and mesencephalon with white matter structures, basal nuclei, thalamus and corpus callosum where included. The exemplary T_1 map of included ROIs can be seen in figure 12.

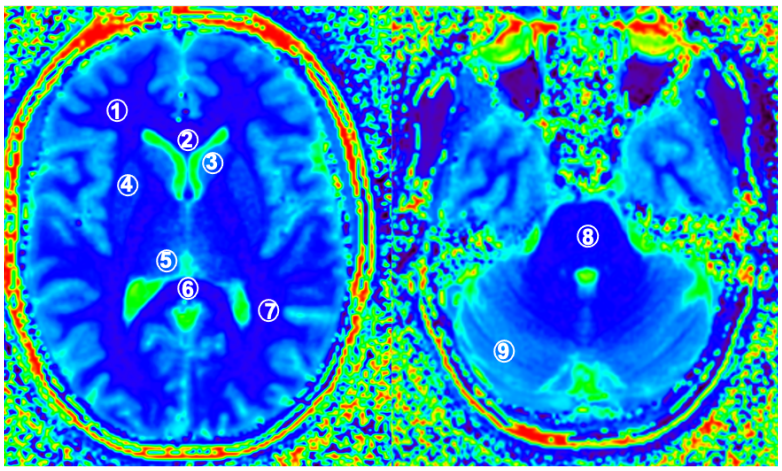

Figure 12: T_1 map with reference ROI placement in patient brain: 1: Frontal white matter, 2: Corpus callosum genu, 3: Nucleus caudatus, 4: Putamen, 5: Thalamus, 6: Corpus callosum splenium, 7: Parietal white matter, 8: Mesencephalon, 9: Cerebellum.

For each study subject, structures of frontal white matter, nucleus caudatus, putamen, thalamus, corpus callosum genu and splenium, parietal white matter, mesencephalon and the cerebellum were examined. Relaxometry values derived from bihemispheric structures (white matter, nucleus caudatus, putamen, thalamus and cerebellar lobe) were averaged for every subject. Structures infiltrated by masses or displaying obvious artifacts were excluded from the analysis. As a result, the number of calculated relaxometry values differs for every anatomic region. In cases where structures of one hemisphere were excluded because of e. g. unilateral tumorous mass infiltration, relaxometry values of the corresponding tissue in the contralateral hemisphere were counted and contributed to the total number of T_1 and T_2 values from the specific anatomic region. The measured numbers of T_1 and T_2 values for each anatomic region can be seen in table 2.

Anatomic region	n (T_1/T_2)
Frontal white matter	87
Corpus callosum genu	69
Nucleus caudatus	82
Putamen	85
Thalamus	84
Corpus callosum splenium	75
Parietal white matter	92
Mesencephalon	84
Cerebellum	85

Table 2: Total number of T_1 and T_2 values measured per anatomic region from the study cohort of 92 patients.

Box plots in figure 13a and c show the distribution of the T_1 and T_2 values of the entire patient cohort revealed by MRF measurements for each anatomic region. For comparison, corresponding box plots from T_1 and T_2 values obtained from the MRF measurements in

the volunteer cohort are shown in figure 13b and d. The absolute mean T_1 relaxation times from the patient measurements vary from around 890 (frontal white matter) to 1348 ms (cerebellum). Small and almost symmetric distributions of T_1 values represented by short boxes with only few outliers are found for white matter structures (frontal and parietal white matter) as well as in the structures of nucleus caudatus, putamen, thalamus and the mesencephalon. Measurements of the frontal white matter for example, show ranging T_1 values from 805.778 ms to 997.831 ms with maximum outliers at 622.154 ms and 1017.0 ms. Similar to the results of the healthy volunteer study, wider distributions and scattered data with a higher number of outliers are found for of the corpus callosum genu and splenium and the cerebellum indicating a large inter-individual variation of the values. T_1 values from the cerebellum for example range from 1139.565 ms to 1555.61 ms with an outlier of 1634.79 ms. For T_2 estimates, the mean values range from around 34 (frontal white matter) to 58 ms (cerebellum). Similar to the T_1 results, small boxes indicating a small data dispersion are derived from white matter structures and basal nuclei. T_2 values of the frontal white matter for example range from 25.666 ms to 43.308 ms with outliers of 21.563 ms and 45.75 ms. A wider dispersion and skewed data is found for T_2 values measured from the cerebellar tissue (range of T_2 values from 36.347 ms to 84.444 ms). The maximum data spread of T_2 values with aberrant outliers exceeding 300 ms is indeed found in the corpus callosum genu (shown in the inset of figure 13b). In general, both T_1 and T_2 relaxometry data obtained from MRF measurements in the patient cohort display wider dispersions and more outliers compared to the T_1 and T_2 data yielded from the healthy volunteer group regardless of the anatomic structure under evaluation.

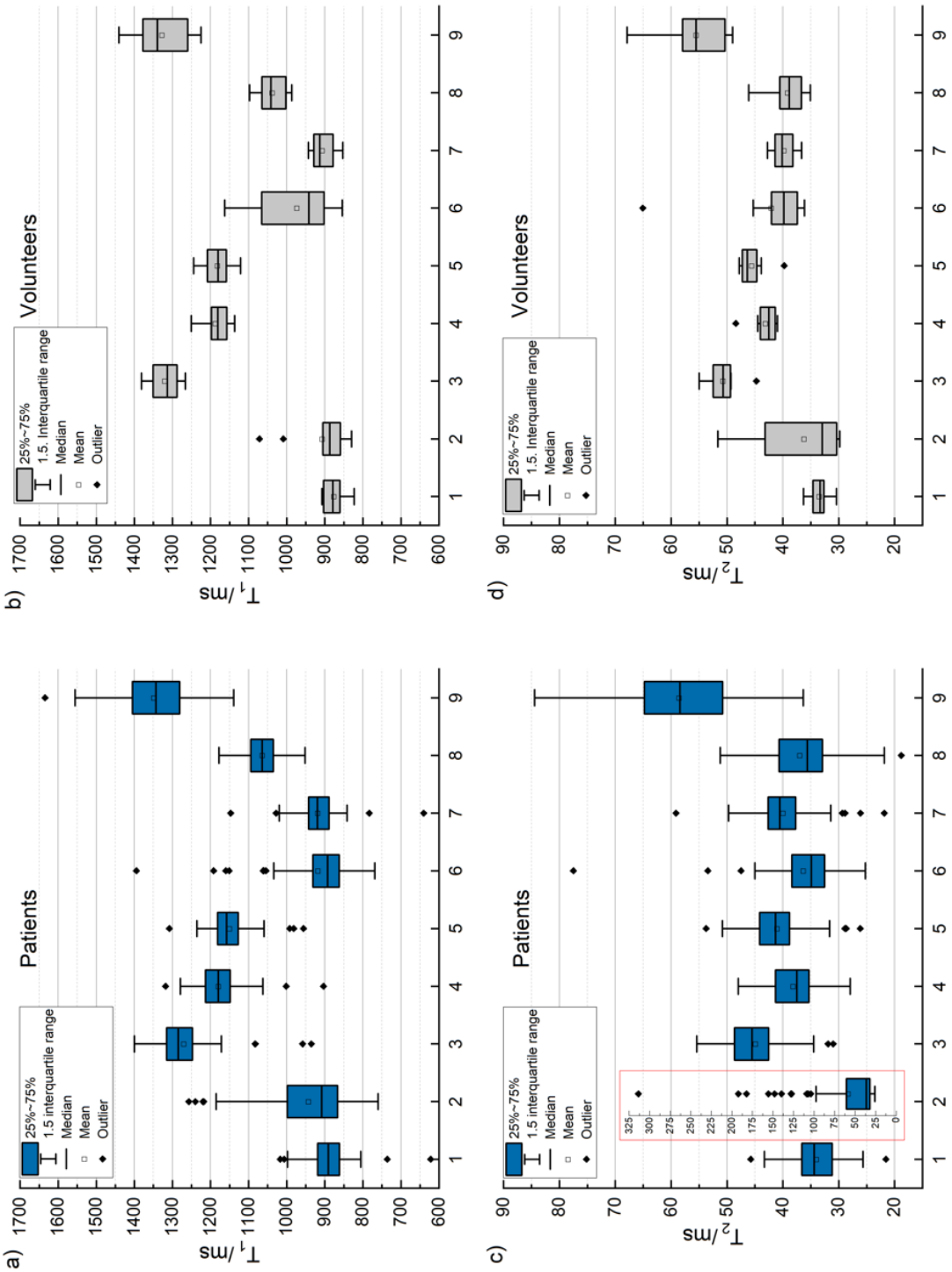

Figure 13: Box plots from T_1 and T_2 values from 9 different anatomic brain regions obtained by MRF at 3 T in a cohort of 92 patients (plot a and c) and in the volunteer cohort (plot b and d, volunteer data taken from chapter 3.2.1). The upper and lower edge of each box indicates the first quartile and third quartile of the data respectively. The inner-box line represents the median and the small square in the box is the mean. The whiskers extend from the top of the box to the maximum data value that is $\leq$ 1.5 times the interquartile range and down from the bottom of the box to the minimum data value that is $>$ 1.5 the interquartile range. All values outside this area are considered as outliers and represented as rhombs. The Inset of plot b shows the box diagram for T_2 data obtained from the structure of corpus callosum genu with aberrant high outliers. X-axis: Anatomic regions 1: Frontal white matter, 2: Corpus call. genu, 3: Nucleus caudatus, 4: Putamen, 5: Thalamus, 6: Corpus call. splenium, 7: Parietal white matter, 8: Mesencephalon, 9: Cerebellum.

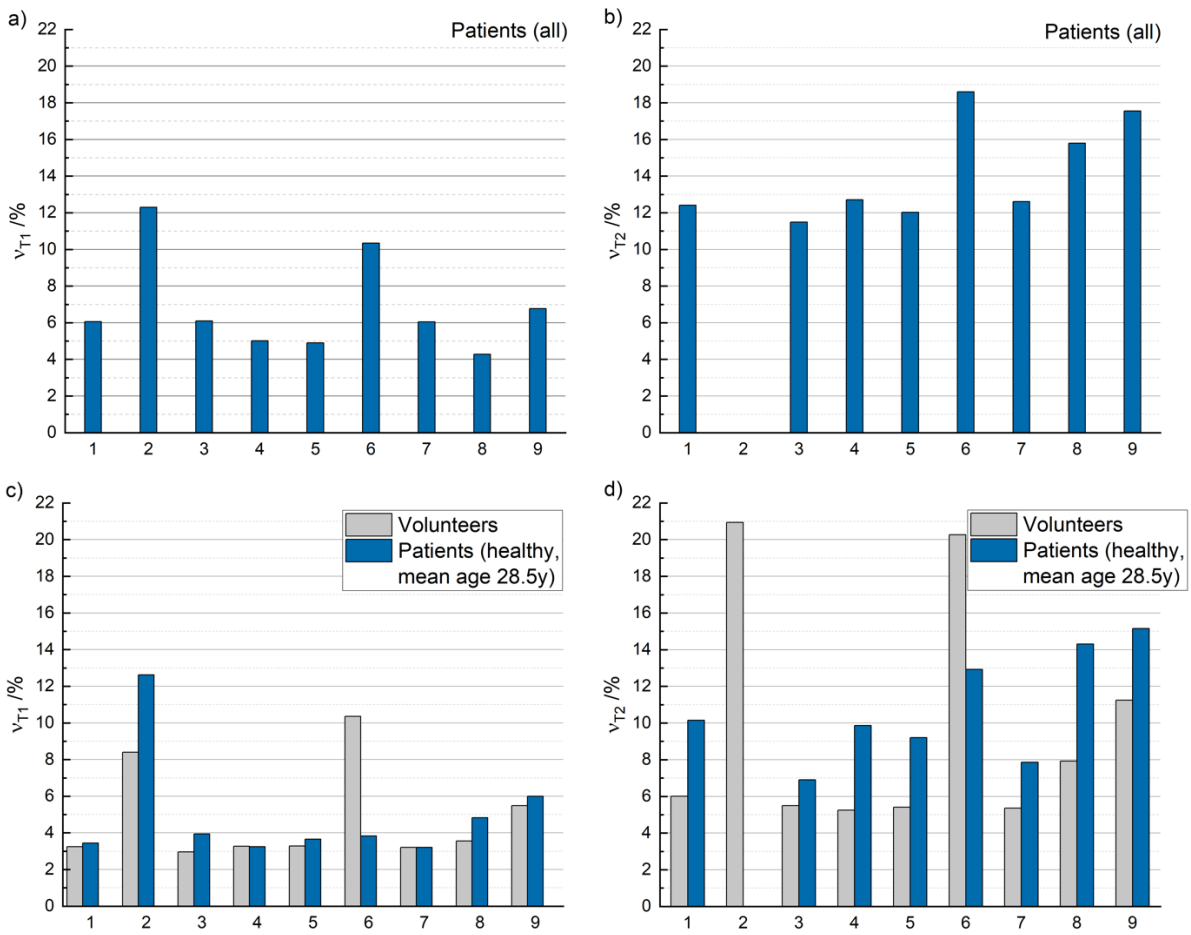

Figure 14: Plot a and b: Repeatability of T_1 and T_2 estimates in 9 different anatomic regions from MRF measurements of the entire patient cohort assessed by the coefficient of variation ν. Plot c and d: Repeatability of T_1 and T_2 values from a sub-group of 10 healthy patients at a mean age of 28.5 ± 4.1 years (blue bars) and the volunteer cohort (gray bars). (For reasons of clarity ν_{T2} from the corpus callosum genu was excluded in plots b and d). X-axis with anatomic regions: 1: Frontal white matter, 2: Corpus call. genu, 3: Nucleus caudatus, 4: Putamen, 5: Thalamus, 6: Corpus call. splenium, 7: Parietal white matter, 8: Mesencephalon, 9: Cerebellum. All results from MRF scans performed in the 3 T scanner system.

Figure 14a and b show the repeatability of T_1 and T_2 estimates from MRF measurements of the entire patient cohort assessed by the coefficients of variation ν_{T1} and ν_{T2}. The highest coefficients of variation in the T_1 data are found in the structures of corpus callosum genu (ν_{T1} = 12.29 %), splenium (ν_{T1} = 10.34 %) and the cerebellum (ν_{T1} = 6.77 %). Small coefficients of variation revealing a low inter-individual variability in the T_1 data are obtained from the putamen (ν_{T1} = 5.01 %), thalamus (ν_{T1} = 4.90 %) and mesencephalon (ν_{T1} = 4.28 %). Regarding the T_2 values the most extreme data variation (ν_{T2} = 86.55 %) is found in the corpus callosum genu as already indicated by aberrant outliers in figure 13c. Similar to the T_1 values, tissues of corpus callosum splenium and the cerebellum yield also higher T_2 data variation in the patient cohort (ν_{T2} = 18.59 % and ν_{T2} = 17.55 % respectively).

Figure 14c and d show the variability of T_1 and T_2 relaxometry values from the volunteer cohort (gray bars) that have been already discussed in chapter 3.2.2, in comparison with the corresponding coefficients of variation calculated from 10 healthy patients (blue bars) at a similar age range as the volunteers (mean age of 28.5 ± 4.1 years, 3 male, 7 female). These 10 patients belong to the sub-group of 26 patients where any kind of brain pathology was excluded via conventional MRI appraisal. T_1 and T_2 values obtained from the entire patient cohort (fig. 14a and b) display higher coefficients of variation for all assessed anatomic structures compared to the results from the volunteer study. In case of the 10 patients with exclusion of any brain pathology and similar age, the data variation is found to be much smaller for both T_1 and T_2 and comparable to the results from the healthy volunteer study. Omitting the corpus callosum genu and splenium the coefficients of variation range from minimum 3.20 % (parietal white matter) to maximum 6.00 % (cerebellum) for T_1, and from minimum 6.89 % (nucleus caudatus) to maximum 15.14 % (cerebellum) for T_2 values from the healthy patient sub-group.

3.3.2 Aging progression of relaxometry data

The progression of T_1 and T_2 relaxometry values with age in the patient collective was evaluated for the white matter structure. The age distribution in the patient cohort was shown in table 1. The absolute T_1 and T_2 relaxometry values for each patient in the frontal white matter tissue in dependence of age is presented in figure 15a and b. T_1 (figure 15a) and T_2 (figure 15b) values from every study subject are calculated as mean values from both hemispheres and ordered by age. A significant positive linear correlation with age is found for T_1 ($p < 0.05$) indicating an increase of longitudinal relaxation time with age. In case of T_2, there is no positive linear correlation and also a polynomial fit does not reveal a significant correlation between transverse relaxation and patient age. A statistically significant relation to age cannot be demonstrated. When mean T_1 and T_2 values are ordered by different age groups the data dispersion for both, T_1 and T_2 values is minimal in the age group of 21 – 30 and comparable to the data dispersion of the T_1 and T_2 values from the volunteer group (see fig. 15c and d). Larger dispersion of the T_1 and T_2 values is found in the higher age groups of patients.

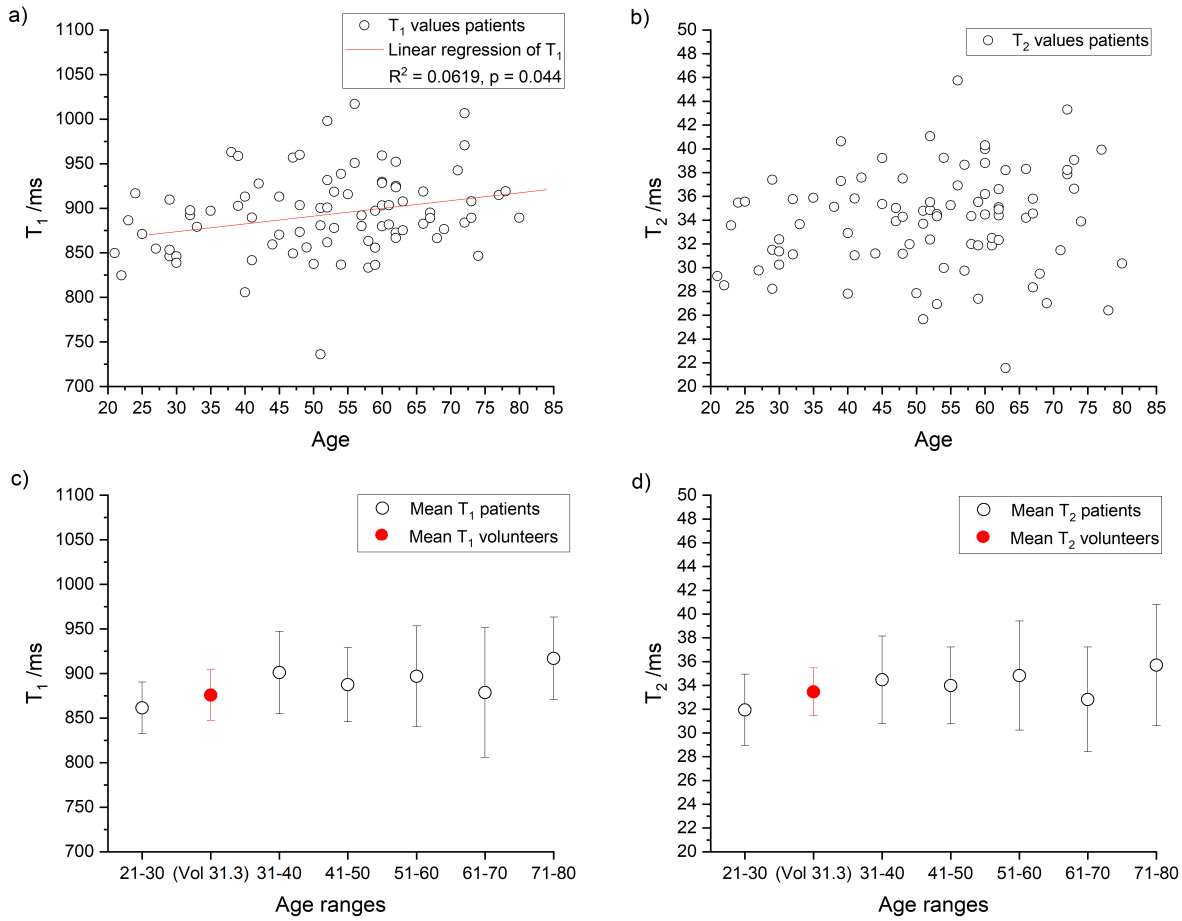

Figure 15: MRF derived T_1 (plot a) and T_2 (plot b) values from the frontal matter structure dependent on the age of the patients at 3 T. Mean T_1 (plot c) and T_2 (plot d) values ordered by different age groups from 21-30 to 71-80 years in comparison to the mean T_1 and T_2 values (red dots in respective plots) calculated from a total of 10 healthy subjects (compare section. 3.2.1). Standard deviations of the relaxometry data in every age group and the volunteer cohort as error bars.

4. Discussion

The goal of the present study was to validate the stability, accuracy and reproducibility of magnetic resonance fingerprinting based on the comparison of phantom scans, scans in healthy volunteers and patients. Our results underline the accuracy and measurement precision of longitudinal and transverse relaxometry estimates from phantom, volunteer and patient studies which yielded consistency with reference data from conventional quantitative imaging tools and previous MR fingerprinting measurements, thus serving as the reference for the application of MRF in clinical routine scans of patients.

4.1 MRF validation in phantom scans

The evaluation of quantitative MRI techniques for stability, reproducibility and accuracy is indispensable before such novel imaging techniques may be implemented into clinical routine imaging. In a first step, the reliability and accuracy of MR fingerprinting was assessed based on repetitive phantom scans and via comparison of the results with existing gold standard NMR techniques.

The inter-scan variability of the T_1 measurement data over 6 successive MRF scans was less than 7 % at both field strengths whereas the variation in T_2 values was notably higher (maximum around 14 % at both 1.5 and 3 T). While higher variation coefficients in T_2 data obtained from MRF measurements have been observed in previous experiments, the reason still remains unclear (Jiang et al. 2017). Overall, reported variations of both T_1 and T_2 relaxometry values derived from gold standard spin echo methods are lower than those observed from MRF. In an earlier repeatability measurement of the ISMRM phantom using spin echo methods over 5 consecutive repetitions the variation of T_1 and T_2 values ranged around 2 % (Jiang et al. 2017). Nevertheless, although these conventional quantitative measurement techniques provide a better repeatability, long acquisition times still prohibit their clinical use. A substantial source of variation in the MRF-derived T_1 and T_2 data may be attributed to the dictionary resolution. A finer step size between two dictionary entries has shown to decrease the standard deviation of T_1 and T_2 values while the accuracy of the values is not affected (Ma et al. 2013; Ma 2015). The repeatability of the measurements could thus be increased by a finer resolved dictionary at the expense of a prolonged computation time.

Mean T_1 values obtained from MRF phantom measurements show a strong correlation with the results from the T_1 data measured with Inversion recovery spin echo methods at both 3 T and 1.5 T. T_2 values also correlate with data obtained from a Carr-Purcell-Meiboom-Gill

sequence at both fields but the relationship does not seem to be linear. In general, both T_1 and T_2 data obtained from MRF bear the tendency to overestimate the values in the shortest NMR-derived T_1 and T_2 time ranges and to underestimate long relaxation times. This is in concordance with an earlier work on MRF-derived relaxometry values from an ISMRM phantom (Jiang et al. 2017). Nevertheless, the MRF results in this work provide overall good correlation with results from conventional mapping sequences in the physiological time ranges of T_1 (100 - 3000 ms) and T_2 (50 - 500 ms) relaxometry data (Badve et al. 2015).

Overall, the phantom experiments show a good repeatability and stability of the MRF technique over repetitive measurements and across a wide range of T_1 and T_2 estimates at both field strengths of 3 T and 1.5 T. The MRF results yielded consistent and reproducible relaxometry estimates compared to results from NMR gold standard methods especially for time ranges reflecting T_1 and T_2 relaxometry values relevant in human brain. This preliminary study validated the accuracy and precision of MRF-derived phantom relaxometry values, hence serving as the reference for the following in-vivo brain measurements.

4.2 MRF validation in healthy volunteers

The volunteer study presented in this work concentrated on the assessment of the stability and repeatability of MRF in an extensive number of brain structures to gain insight into the overall transferability of MRF from phantom scans to human tissue. The imaging slices were chosen in a way that the resulting T_1 and T_2 estimates provide a complete quantitative characterization of the most important brain structures with respect to typical locations of structural brain diseases. Until initiation of this study only a few brain structures like white and gray matter, thalamus and few deep brain structures were addressed and characterized by conventional quantitative relaxometry measurements (Whittall et al. 1997; Deoni et al. 2005; Lu et al. 2005). As the most common cerebral metastases and primary brain tumors are known to be located in the cerebral hemispheres (Ostrom et al. 2015), one focus of the measurements in our study was put on white matter which was assessed based on a multi-ROI analysis over three different levels. Furthermore, deep brain structures such as basal nuclei and the thalamus were also studied, as these structures are known to be of high clinical importance. In these regions, especially histologic extirpation or targeted tumor therapy still remains challenging and complex. A comprehensive characterization by quantitative imaging parameters may improve diagnosis and therapy of diseases affecting these structures.

Overall, our study results in healthy volunteers demonstrate the transferability of phantom scans to in vivo MRF imaging, as only small T_1 and T_2 data dispersions in white matter, thalamus and basal nuclei were shown.

4.2.1 Comparison to conventional mapping techniques and initial MRF results

The relaxometry measurements in the study population of 10 healthy volunteers also yielded consistent results compared to conventional relaxometry mapping strategies found in literature as shown in table 3 and 4 of the supplementary material in chapter 7.1. T_1 values found in literature are generally based on inversion recovery methods (Carr and Purcell 1954; Whittall et al. 1997; Deoni et al. 2005; Lu et al. 2005). Published T_2 estimates are usually determined from (multiple) spin-echo sequences like the Carl-Purcell-Meiboom-Gill (CPMG) sequence (Meiboom and Gill 1958; Lu et al. 2005). A large variability of reported T_1 and T_2 values measured in 3 T and 1.5 T scanner systems is evident from all structures that were accessed by different quantitative imaging methods and sequences. Overall, the mean MRF-derived T_1 and T_2 estimates obtained from white and gray matter and basal nuclei structures in this work lie within the range of the reported literature values. However, the broad extent of previously reported relaxometry data seen in table 3 and 4 (supplementary material, section 7.1.1) contradicts a dedicated confinement of the range of physiologic i. e. universal T_1 and T_2 relaxation values for more accurate comparison. The reported relaxometry values are derived from different imaging methods and sequences which leads to a large inter-study variability (Bojorquez et al. 2017). Technical issues such as different scanner systems, scanner performance and modalities as well as number of scanned subjects have to be considered as a source of data variability. Additionally, differences in study design, number and condition of scanned subjects, scanner hardware, sequence design and data acquisition are factors that have to be taken into account when comparing data from different imaging setups. Moreover, issues of noise present in the received signal, partial volume- and B_1-effects and transverse coherences or spoiling cause systematic errors that also affect the accuracy of relaxometry data compared in tables 3 and 4 (Bojorquez et al. 2017). All these factors complicate an objective comparison of quantitative relaxometry values. Although the broad extent of these literature values derived from different inversion recovery and spin echo methods contradict particular/universal T_1 and T_2 reference values, an overall good concordance of the literature data with MRF results from the present work can be concluded.

A comparison of mean relaxometry estimates with preliminary MRF measurements published in 2013 and 2019 at the Case Western Reserve University yielded also consistent

results (see table 5, supplemental material, section 7.1.2) (Ma et al. 2013; Ma et al. 2019). Especially relaxometry values obtained at 3 T yield commensurable results with only 4 to 7 % difference on an average between measured T_1 and T_2 values. Nevertheless, in some cerebral regions a larger deviation of 12.74 % for T_1 (centrum semiovale at 3 T) and 16.79 % and 37.94 % for T_2 (frontal white matter at 3 T, frontal white matter at 1.5 T) from the corresponding published results is obtained. Apart from hardware and software differences, a missing B_1-correction in former MRF implementations can be discussed as one reason for the observed larger deviation (Jiang et al. 2017).

4.2.2 Discussion of data variability

The inter-individual variability of relaxometry measurements (figure 11) between 10 healthy subjects did not exceed 6 % for T_1 and 15 % for T_2 at both field strengths omitting values from cortical gray matter, corpus callosum and splenium. Relaxometry data from these structures vary up to 10 % for T_1 and more than 20 % for T_2 at both 1.5 and 3 T (figure 11). Particularly the higher variation coefficients from the corpus callosum genu and splenium may be attributed to slight inaccuracies regarding the slice height adjustment during the scanning procedure. Larger variation in relaxometry estimates of cortical gray matter parameters are supposed to mainly arise from partial volume effects, due to multi-component contributions to the voxels (Ballester et al. 2002; Deshmane et al. 2019). Measurements of cortical and sub-cortical grey matter display mixed voxels composed of a mixture of different tissue types with fractional amount of cerebrospinal fluid or white matter in the same region due to the limited spatial resolution of the imaging modality, leading to variations in the MR signal intensity. The signal evolution is affected not only by the imaging sequence and tissue property of the voxel but also depends on the portion of each tissue in the voxel that can lead to significant errors and thus inter-individual deviation in quantitative measurements (Ballester et al. 2000). The overall larger variations in T_2 measurements are accordant to recently reported findings from multiple repetitive in vivo MRF scans but the origin still remains unclear (Körzdorfer et al. 2019).

The coefficients of variation for both T_1 and T_2 estimates shown in the healthy volunteer study are higher compared to the inter-scan variability results found in repetitive phantom scans at both field strengths (compare section 3.1). Besides the specific factors mentioned above, the higher variability may also be attributed to the presumptive factor that imaging a human brain is more complex than scanning a phantom in terms of field-of-view positioning or heterogeneity of the region under study. Physiological issues such as gender and left- or right-handedness have also shown to affect the ranges of relaxometry estimates but were

not taken into account in this examination of the participants. These factors can limit reproducibility when compared to phantom measurements. Nevertheless, when omitting the results from structures of the corpus callosum genu and splenium, the coefficients of variation from both T_1 and T_2 found for all other anatomic regions do not exceed the maximum T_1 and T_2 variations measured from the ISMRM phantom independent of the field strength. Thus, the volunteer scans revealed one of the first in-vivo implementations of MRF as a rapid multiparametric quantification tool of normative brain relaxometry data from multiple brain regions with a sufficient accuracy, robustness and reproducibility.

4.3 MRF validation in patients

Given the rather short acquisition and reconstruction times of less than a minute, the MRF protocol was successfully integrated into the daily clinical imaging workflow of the department of Radiology at the University Hospital Essen. All MRF scans were performed at a 3 T scanner within the scope of every patient's conventional imaging protocol and prior to the application of contrast agent. The additional MRF scans were well tolerated by all subjects. The scanning procedures were smoothly integrated into the clinical workflows at minimal extra time required for involved medical and technical staff.

3 Tesla MRI has evolved to become the field strength of choice for neuroimaging as well as musculoskeletal imaging. The advantages of higher field strength comprise an increased signal-to-noise ratio and better spatial resolution (Lu et al. 2005; Baudendistel et al. 2004). Hence, in adherence to our clinical workflow of performing 3 T scans for neuroimaging, the investigations on MRF in patients were limited to 3 T scans in this study.

While the volunteer study attempted to investigate as many different anatomic regions as possible, few anatomic regions had to be omitted from the ROI analysis in the patient collective in order to guarantee a fluent and reliable quantitative evaluation and analysis routine. Exact quantification of structures like the vermis, internal capsule or corpus callosum suffered from slight variations in the field-of-view positioning. Aberrant outliers in the T_2 dataset and corresponding high variation coefficients found in the corpus callosum genu may be most probably attributed to known additional banding and susceptibility artifacts. As already discussed in the previous section, MRF is also susceptible to artifacts arising from the partial volume effect that seem to have a considerable impact especially on gray matter structures (Pierre et al. 2016; McGivney et al. 2018). Therefore, anatomic regions of gray matter, internal capsule and vermis have been omitted from the actual analysis of the patient data. The number of white matter structures under investigation was

also reduced for reasons of analysis time efficiency since the ROI analysis was done manually by a research assistant during the period of patient scans.

Relaxometry estimates obtained from the patient data displayed a larger dispersion and higher variation coefficients than those obtained from healthy subjects. Higher variation in the data from the patient collective may be primarily attributed to the wider age spread in the cohort. It became evident that relaxometry parameters in human brain change during aging progression based on physiological and mostly microstructural changes in different brain regions like cerebral white and gray matter (Ge et al. 2002; Hsu et al. 2008). In particular, irreversible damage of fiber myelin, increase in gliosis and free water content and the loss of axons and synaptic terminals characterize cerebral aging processes (Kennedy and Raz 2009; Pannese 2011; Callaghan et al. 2014). These findings directly relate to changes in the relaxometry parameters with age. Motion artifacts are also suggested to have a higher impact on the patient measurements leading to a larger data variability than in the volunteer group. Old, multimorbid and agitated patients or patients with psychological issues such as anxiety or claustrophobia are suggested to probably move more during an MR scan than healthy study participants which can lead to significant motion artifacts.

Nevertheless, T_1 and T_2 data from a patient subgroup at the same age range as the healthy volunteer group and exclusion of any brain pathology revealed low and comparable coefficients of variation as the volunteer measurements, confirming the stability and reproducibility of the MRF method over a period of 6 months.

The focus on an accurate characterization of imaging parameters within aging progression could be of particular interest in the diagnosis and therapy of diseases related essentially to the elderly. Previous works on conventional quantitative mapping techniques have shown that measurements of relaxometry values can be principally used to identify subtle microstructural changes for example in early Alzheimer's disease before significant brain tissue atrophy occurs (Wearn et al. 2020). Examination of such minimal pathologic changes via quantitative mapping techniques requires accurate and stable imaging parameters, so that subtle variations from the norm in a specific tissue can be confidently attributed to pathology. In concordance with previous studies on the relationship of relaxometry values and age in human brain, MRF-derived T_1 values in the frontal white matter show a significant increase with age representing structural changes in cerebral neurons, myelin or decrease of cellular substance with aging. In contrast, a significant relationship between T_2 values and age in white matter could not be obtained in this work. Previous works regarding the age relation of T_2 have shown inconsistent results. T_2 values in white matter obtained from spin echo methods yielded either no significant correlation or a weak linear correlation with

age (Agartz et al. 1991; Breger et al. 1991). A former study on age relation of MRF-derived relaxometry values showed a linear correlation in the left and a quadratic relationship of T_2 in the right frontal white matter (Badve et al. 2015). All in all, the age relation of transverse relaxation remains unclear.

4.4 Limitations

In order to be fully integrated and be able to set new standards in the clinical workflow the MRF technique needs to be optimized. Important remaining challenges can be divided in two main sections including technical parts and issues of experimental setup, patient recruitment and scanning routine.

As already discussed in section 1.4.2, the dictionary resolution of the MRF implementation can limit the quality of the measured values leading to a reduced stability and repeatability. Additionally, a finer dictionary step size that could enable more accurate measurements, increases the computation time simultaneously as a trade-off. Recent publications addressing novel post-processing methods like fast group matching techniques and the use of a compressed dictionary for MRF show that the repeatability of MRF parameter mapping can be increased without extending the computation time (McGivney et al. 2014; Cauley et al. 2015).

Since the results of this work belong to a research field with only a small number of publications on this topic, the role of pathologies which affect the human brain in a global manner remains unclear. Relaxometry values contributing to this study were extracted from ROIs including only visually normal tissue. Only tumor- or artifact-free areas were investigated whereas the history of various endocrinopathies, hypertension or drug intake which can affect brain tissue in a global manner remained disregarded (Rodrigue et al. 2011; Pell et al. 2012; Bagga et al. 2015). In order to establish a database with quantitative relaxometry data covering and characterizing normal brain tissue, attention should be drawn to multicenter investigations of global changes affecting these parameters.

The imaging workflow in the current in vivo studies requires accurate slice adjustment in order to obtain reliable and reproducible results. During the 6-month study period many different radiology technicians were involved in the patient scans. Experimental settings and program adjustments vary with the technician teams and may lead to systematical errors/inconsistencies. Especially, slight variations in manual slice placement may have led to non-uniform mapping of certain structures in some of the study subjects. Automated slice

placement could provide objective and more standardized selection of brain levels throughout the whole cohort and accelerate imaging workflows with each subject.

The efficient and fluent analysis of larger patient cohorts is currently limited by non-automatized data evaluation including manual ROI analysis. Selecting and drawing ROIs by hand depends on the radiologists' or research assistants' experience. Depending on the number of ROIs, this selection procedure can be very time consuming. An alternative annotation method based on symmetric diffeomorphic image registration for automatic data evaluation has been tested on asymptomatic volunteers in order to improve ROI analysis and database organization (Avants et al. 2008).

4.5 Conclusion

MRF is feasible in phantoms, healthy volunteers, and patients. The present work showed a fast and accurate estimation of quantitative relaxometry data in the human brain using MRF. Longitudinal and transverse relaxometry measurements obtained from MRF showed highly stable and repeatable results in an ISMRM/NIST phantom and a healthy volunteer cohort. After validation in an imaging phantom and healthy volunteers, the MRF protocol was successfully integrated into the daily clinical imaging workflow and MRF measurements were launched in a large patient cohort of 92 subjects. Relaxometry estimates obtained from the patient data displayed a larger dispersion and higher variation coefficients than those obtained from healthy subjects. Higher variation in the data from the patient collective may be primarily attributed to the wider age spread with according physiological changes in the brain tissue in this cohort. T_1 and T_2 data from a sub-group of patients at the same age range as the healthy volunteer group revealed comparable coefficients of variation as the volunteer measurements, confirming the long-term stability and reproducibility of the MRF method over a period of several months. The quantification of normative brain tissue parameters from the large patient cohort shown in this work could contribute to a wider comprehensive clinical reference data base of normative relaxometry data in order to establish tissue relaxometry as reliable non-invasive biomarkers and improve diagnostics in neuroimaging.

5. Summary/ Zusammenfassung

Magnetic Resonance Fingerprinting (MRF) was recently introduced as a novel approach to fast quantitative Magnetic Resonance Imaging (MRI) that allows simultaneous and efficient measurement of multiple tissue properties during one single, rapid acquisition. The aim of this work was to estimate the stability and accuracy of the MRF framework in an imaging phantom and non-pathologic brain tissue from healthy volunteers and a large patient collective by measurements of longitudinal (T_1) and transverse (T_2) relaxation times at field strengths of 1.5 and 3 T. A goal was also to investigate the options to integrate MRF into routine workflows of neuroimaging in the clinical setting.

Repetitive phantom scans yielded stable and reproducible results across a wide range of relaxometry values with coefficients of variation less than 7 % for T_1 and less than 14 % for T_2 estimates at both field strengths. Linear correlation of MRF results and relaxometry data obtained by Nuclear Magnetic Resonance (NMR) measurements validated the accuracy of the MRF method in vitro. MRF relaxometry measurements of various brain tissues in a study population of 10 healthy volunteers were in sufficient agreement with conventional quantitative imaging techniques and previous MRF data found in literature. The inter-individual variability of relaxometry measurements obtained from multiple structures of white matter, basal nuclei and thalamus showed maximum values of 6 % for T_1 and 15 % for corresponding T_2 measurements at 1.5 and 3 T, confirming an adequate repeatability of the MRF method in vivo. After validation of phantom and volunteer measurements, MRF scans were successfully integrated into the clinical workflow. Within a time period of six month, 92 patients with either previously diagnosed neurological pathologies or suspected diagnosis of brain pathologies that were scheduled for a routine clinical MRI protocol at 3 T received an additional MRF brain scan. From anatomical regions that were not infiltrated by pathology MRF relaxometry values were compared across subjects and to corresponding results in healthy volunteers. In general, T_1 and T_2 estimates obtained from patient data showed higher variation coefficients than those in healthy subjects. This may be primarily attributed to the wider spread in age and larger impact of motion artifacts in the patient cohort. The comparison of relaxometry values from a sub-group of 10 patients at the same age range as the healthy volunteers revealed similar low coefficients of variation as found in the volunteer cohort, thus confirming the long-term stability of the MRF measurements over several months.

Obtained relaxometry data from multiple healthy brain structures may contribute to a normative database of MRF relaxometry estimates that could help to establish quantitative imaging biomarkers for improvement of diagnostics in neuroimaging.

Das vor Kurzem entwickelte Magnetresonanz-Fingerprinting-Verfahren (MRF) stellt einen neuartigen Ansatz einer quantitativen Gewebeklassifizierung auf dem Gebiet der Magnetresonanztomographie (MRT) dar und erlaubt eine effiziente und simultane Messung multipler Gewebeparameter. Das Ziel dieser Arbeit war es, die Präzision und Wiederholbarkeit der MRF-Methode anhand von longitudinalen (T_1) und transversalen (T_2) Relaxationszeitmessungen eines Testphantoms und gesundem Hirngewebe in einer Probandengruppe sowie in einer großen Patientenkohorte zu ermitteln. Darüber hinaus bestand ein Ziel darin, Möglichkeiten der Einbindung der MRF-Applikation in die klinischen Arbeitsabläufe der neuroradiologischen Bildgebung zu eruieren.

Repetitive MRF-Messungen des Testphantoms bei Feldstärken von 1.5 und 3 T zeigten stabile und reproduzierbare Ergebnisse der Relaxationszeiten mit Variationskoeffizienten von weniger als 7 % für T_1- und weniger als 14 % für T_2-Werte. Eine lineare Korrelation von MRF-basierten Relaxationszeiten und etablierten kernspinresonanzbasierten (NMR) Messungen bestätigte die Präzision des MRF-Verfahrens in-vitro. MRF-Relaxationszeitmessungen multipler Hirnstrukturen in einer Studienpopulation mit 10 gesunden Probanden waren vergleichbar mit entsprechenden Ergebnissen konventioneller quantitativer MRT-Verfahren und früheren MRF-Messungen aus der Literatur. Die interindividuelle Variabilität der Relaxationszeiten – ermittelt in den Strukturen der weißen Substanz, den Basalganglien und des Thalamus bei 1.5 und 3 T – betrug maximal 6 % für T_1- und maximal 15 % für T_2-Werte, womit eine adäquate Wiederholbarkeit der MRF-Messungen in-vivo nachgewiesen werden konnte. Innerhalb eines Zeitraums von sechs Monaten erhielten 92 Patienten mit neurologischen Erkrankungen oder entsprechenden Verdachtsdiagnosen im Rahmen ihrer geplanten konventionellen MRT-Untersuchung zusätzlich einen MRF-Scan des Kopfes bei 3 T. Die gemessenen T_1- und T_2-Werte von ausschließlich gesunden Hirngewebestrukturen innerhalb der Patientenkohorte zeigten insgesamt eine höhere interindividuelle Variabilität verglichen mit den Resultaten der Probandengruppe. Dies kann vornehmlich mit der breiteren Altersverteilung der Patientenkohorte sowie vermehrten Bewegungsartefakten bei den Patientenscans assoziiert werden. Die Variabilität der T_1- und T_2-Werte innerhalb einer Subgruppe von 10 Patienten im ähnlichen Alter wie die Probanden war hingegen geringer und vergleichbar mit den Ergebnissen der Probandengruppe. Dieses Ergebnis unterstreicht die Stabilität und Reproduzierbarkeit der MRF-Methode über einen längeren Zeitraum von mehreren Monaten. Die gezeigten Ergebnisse der Relaxationszeitmessungen multipler Hirnstrukturen könnten dazu beitragen, eine Referenzdatenbank MRF-basierter Gewebeparameter einzurichten, um quantitative Biomarker zur Entwicklung und Optimierung diagnostischer Verfahren in der Neuroradiologie zu etablieren.

6. Bibliography

1. Agartz, I., Sääf, J., Wahlund, L. O., Wetterberg, L. (1991): T1 and T2 relaxation time estimates in the normal human brain. Radiology 181, 537-543.

2. Avants, B. B., Epstein, C. L., Grossman, M., Gee, J. C. (2008): Symmetric diffeomorphic image registration with cross-correlation: evaluating automated labeling of elderly and neurodegenerative brain. Med Image Anal 12, 26-41.

3. Badve, C., Yu, A., Rogers, M., Ma, D., Liu, Y., Schluchter, M., Sunshine, J., Griswold, M., Gulani, V. (2015): Simultaneous T(1) and T(2) Brain Relaxometry in Asymptomatic Volunteers using Magnetic Resonance Fingerprinting. Tomography 1, 136-144.

4. Bagga, D., Modi, S., Poonia, M., Kaur, P., Bhattacharya, D., Garg, M. L., Khushu, S., Singh, N. (2015): T2 relaxation time alterations underlying neurocognitive deficits in alcohol-use disorders (AUD) in an Indian population: A combined conventional ROI and voxel-based relaxometry analysis. Alcohol 49, 639-646.

5. Ballester, M. A. G., Zisserman, A., Brady, M. (2000): Segmentation and measurement of brain structures in MRI including confidence bounds. Med Image Anal 4, 189-200.

6. Ballester, M. A. G., Zisserman, A. P., Brady, M. (2002): Estimation of the partial volume effect in MRI. Med Image Anal 6, 389-405.

7. Baudendistel, K. T., Heverhagen, J. T., Knopp, M. V. (2004): Klinische MRT bei 3 Tesla: Aktueller Stand. Der Radiologe 44, 11-18.

8. Bitar, R., Leung, G., Perng, R., Tadros, S., Moody, A. R., Sarrazin, J., McGregor, C., Christakis, M., Symons, S., Nelson, A., Roberts, T. P. (2006): MR pulse sequences: what every radiologist wants to know but is afraid to ask. Radiographics 26, 513-537.

9. Bloch, F. (1946): Nuclear Induction. Physical Review 70, 460-474.

10. Bojorquez, J. Z., Bricq, S., Acquitter, C., Brunotte, F., Walker, P. M., Lalande, A. (2017): What are normal relaxation times of tissues at 3 T?, Magn Reson Imaging 35, 69-80.

11. Breger, R. K., Yetkin, F. Z., Fischer, M. E., Papke, R. A., Haughton, V. M., Rimm, A. A. (1991): T1 and T2 in the cerebrum: correlation with age, gender, and demographic factors. Radiology 181, 545-547.

12. Buonincontri, G., Sawiak, S. J. (2016): MR fingerprinting with simultaneous B1 estimation. Magn Reson Med 76, 1127-1135.

13. Callaghan, M. F., Freund, P., Draganski, B., Anderson, E., Cappelletti, M., Chowdhury, R., Diedrichsen, J., Fitzgerald, T. H., Smittenaar, P., Helms, G., Lutti, A., Weiskopf, N. (2014): Widespread age-related differences in the human brain microstructure revealed by quantitative magnetic resonance imaging. Neurobiol Aging 35, 1862-1872.

14. Carr, H. Y., Purcell, E. M. (1954): Effects of Diffusion on Free Precession in Nuclear Magnetic Resonance Experiments. Physical Review 94, 630-638.

15. Cauley, S. F., Setsompop, K., Ma, D., Jiang, Y., Ye, H., Adalsteinsson, E., Griswold, M. A., Wald, L. L. (2015): Fast group matching for MR fingerprinting reconstruction. Magn Reson Med 74, 523-528.

16. Coppo, S., Mehta, B. B., McGivney, D., Ma, D., Chen, Y., Jiang, Y., Hamilton, J., Pahwa, S., Badve, C., Seiberlich, N., Griswold, M., Gulani, V. (2016): Overview of Magnetic Resonance Fingerprinting. MAGNETOM flash 1, 12-21.

17. Crawley, A. P., Henkelman, R. M. (1988): A comparison of one-shot and recovery methods in T1 imaging. Magn Reson Med 7, 23-34.

18. Dale, B. M., Brown, M. A., Semelka, R. C. (2015): MRI: Basic Principles and Applications. 5. Ed. West Sussex: Wiley Blackwell.

19. Deoni, S. C. (2010): Quantitative relaxometry of the brain. Top Magn Reson Imaging 21, 101-113.

20. Deoni, S. C., Peters, T. M., Rutt, B. K. (2005): High-resolution T1 and T2 mapping of the brain in a clinically acceptable time with DESPOT1 and DESPOT2. Magn Reson Med 53, 237-241.

21. Deoni, Sean C.L., Rutt, Brian K., Peters, Terry M. (2003): Rapid combined T1 and T2 mapping using gradient recalled acquisition in the steady state. Magnetic Resonance in Medicine 49, 515-526.

22. Deshmane, Anagha, McGivney, Debra F., Ma, Dan, Jiang, Yun, Badve, Chaitra, Gulani, Vikas, Seiberlich, Nicole, Griswold, Mark A. (2019): Partial volume mapping using magnetic resonance fingerprinting. NMR in Biomedicine 32, e4082.

23. Doneva, M., Börnert, P., Eggers, H., Stehning, C., Sénégas, J., Mertins, A. (2010): Compressed sensing reconstruction for magnetic resonance parameter mapping. Magn Reson Med 64, 1114-1120.

24. Dougherty, D. D., Rauch, S. L., Rosenbaum, J. F. (2004): Essentials of Neuroimaging for Clinical Practice. Washington, D.C., London: American Psychiatric Publishing, Inc.

25. Ghugre, N. R., Ramanan, V., Pop, M., Yang, Y., Barry, J., Qiang, B., Connelly, K. A., Dick, A. J., Wright, G. A. (2011): Quantitative tracking of edema, hemorrhage, and microvascular obstruction in subacute myocardial infarction in a porcine model by MRI. Magn Reson Med 66, 1129-1141.

26. Grover, V. P., Tognarelli, J. M., Crossey, M. M., Cox, I. J., Taylor-Robinson, S. D., McPhail, M. J. (2015): Magnetic Resonance Imaging: Principles and Techniques: Lessons for Clinicians. J Clin Exp Hepatol 5, 246-255.

27. Hahn, E. L. (1950): Spin Echoes. Physical Review 80, 580-594.

28. Hargreaves, B. A., Nishimura, D. G., Conolly, S. M. (2004): Time-optimal multidimensional gradient waveform design for rapid imaging. Magnetic Resonance in Medicine 51, 81-92.

29. Hsieh, J. J. L., Svalbe, I. (2020): Magnetic resonance fingerprinting: from evolution to clinical applications. Journal of Medical Radiation Sciences 67, 333 - 344.

30. Huang, T. Y., Liu, Y. J., Stemmer, A., Poncelet, B. P. (2007): T2 measurement of the human myocardium using a T2-prepared transient-state TrueFISP sequence. Magn Reson Med 57, 960-966.

31. Jiang, Y., Ma, D., Keenan, K. E., Stupic, K. F., Gulani, V., Griswold, M. A. (2017): Repeatability of magnetic resonance fingerprinting T(1) and T(2) estimates assessed using the ISMRM/NIST MRI system phantom. Magn Reson Med 78, 1452-1457.

32. Jiang, Y., Ma, D., Seiberlich, N., Gulani, V., Griswold, M. A. (2015): MR fingerprinting using fast imaging with steady state precession (FISP) with spiral readout. Magn Reson Med 74, 1621-1631.

33. Just, M., Thelen, M. (1988): Tissue characterization with T1, T2, and proton density values: results in 160 patients with brain tumors. Radiology 169, 779-785.

34. Keenan, K. E., Ainslie, M., Barker, A. J., Boss, M. A., Cecil, K. M., Charles, C., Chenevert, T. L., Clarke, L., Evelhoch, J. L., Finn, P., Gembris, D., Gunter, J. L., Hill, D. L. G., Jack, C. R., Jr., Jackson, E. F., Liu, G., Russek, S. E., Sharma, S. D., Steckner, M., Stupic, K. F., Trzasko, J. D., Yuan, C., Zheng, J. (2018): Quantitative magnetic resonance imaging phantoms: A review and the need for a system phantom. Magn Reson Med 79, 48-61.

35. Keenan, K. E., Wilmes, L. J., Aliu, S. O., Newitt, D. C., Jones, E. F., Boss, M. A., Stupic, K. F., Russek, S. E., Hylton, N. M. (2016): Design of a breast phantom for quantitative MRI. J Magn Reson Imaging 44, 610-619.

36. Keenan, K., Stupic, K., Boss, M., Russek, S., Chenevert, T., Prasad, P., Reddick, W., Zheng, J., Hu, P., Jackson, E. (2016): "Comparison of T1 measurement using ISMRM/NIST system phantom." In Proceedings of the International Society of Magnetic Resonance in Medicine. ISMRM 24th Annual Meeting, Singapore.

37. Kennedy, K. M., Raz, N. (2009): Pattern of normal age-related regional differences in white matter microstructure is modified by vascular risk. Brain Res 1297, 41-56.

38. Körzdorfer, G., Kirsch, R., Liu, K., Pfeuffer, J., Hensel, B., Jiang, Y., Ma, D., Gratz, M., Bar, P., Bogner, W., Springer, E., Lima Cardoso, P., Umutlu, L., Trattnig, S., Griswold, M., Gulani, V., Nittka, M. (2019): Reproducibility and Repeatability of MR Fingerprinting Relaxometry in the Human Brain. Radiology 292, 429-437.

39. Lemasson, B., Pannetier, N., Coquery, N., Boisserand, Ligia S. B., Collomb, Nora, Schuff, N., Moseley, M., Zaharchuk, G., Barbier, E. L., Christen, T. (2016): MR Vascular Fingerprinting in Stroke and Brain Tumors Models. Scientific Reports 6, 37071.

40. Look, D. C., Locker, D. R. (1970): Time Saving in Measurement of NMR and EPR Relaxation Times. Review of Scientific Instruments 41, 250-251.

41. Lu, H., Nagae-Poetscher, L. M., Golay, X., Lin, D., Pomper, M., van Zijl, P. C. (2005): Routine clinical brain MRI sequences for use at 3.0 Tesla. J Magn Reson Imaging 22, 13-22.

42. Lugauer, F., Wetzl, J. (2018): Magnetic Resonance Imaging. In: Maier, A., Steidl, S., Christlein, V., Hornegger, J. (Eds.): Medical Imaging Systems: An Introductory Guide. Pp. 91-109. Cham (CH): Springer International Publishing.

43. Ma, D. (2015): Magnetic Resonance Fingerprinting. Doctoral dissertation, Case Western Reserve University School of Graduate Studies. Cleveland, Ohio.

44. Ma, D., Gulani, V., Seiberlich, N., Liu, K., Sunshine, J. L., Duerk, J. L., Griswold, M. A. (2013): Magnetic resonance fingerprinting. Nature 495, 187-192.

45. Ma, D., Jones, S. E., Deshmane, A., Sakaie, K., Pierre, E. Y., Larvie, M., McGivney, D., Blümcke, I., Krishnan, B., Lowe, M., Gulani, V., Najm, I., Griswold, M. A., Wang, Z. I. (2019): Development of high-resolution 3D MR fingerprinting for detection and characterization of epileptic lesions. J Magn Reson Imaging 49, 1333-1346.

46. Ma, D., Pierre, E. Y., Jiang, Y., Schluchter, M. D., Setsompop, K., Gulani, V., Griswold, M. A. (2016): Music-based magnetic resonance fingerprinting to improve patient comfort during MRI examinations. Magn Reson Med 75, 2303-2314.

47. McGivney, D., Deshmane, A., Jiang, Y., Ma, D., Badve, C., Sloan, A., Gulani, V., Griswold, M. (2018): Bayesian estimation of multicomponent relaxation parameters in magnetic resonance fingerprinting. Magn Reson Med 80, 159-170.

48. McGivney, D. F., Pierre, E., Ma, D., Jiang, Y., Saybasili, H., Gulani, V., Griswold, M. A. (2014): SVD compression for magnetic resonance fingerprinting in the time domain. IEEE Trans Med Imaging 33, 2311-2322.

49. McSheehy, P. M., Weidensteiner, C., Cannet, C., Ferretti, S., Laurent, D., Ruetz, S., Stumm, M., Allegrini, P. R. (2010): Quantified tumor t1 is a generic early-response imaging biomarker for chemotherapy reflecting cell viability. Clin Cancer Res 16, 212-225.

50. Mehta, B., Coppo, S., McGivney, D., Hamilton, J., Chen, Y., Jiang, Y., Ma, D., Seiberlich, N., Gulani, V., Griswold, M. (2019): Magnetic resonance fingerprinting: a technical review. Magn Reson Med 81, 25-46.

51. Meiboom, S., Gill, D. (1958): Modified Spin-Echo Method for Measuring Nuclear Relaxation Times. Review of Scientific Instruments 29, 688-691.

52. NIST, National Institute of Standards and Technology. (2016). https://www.nist.gov/programs-projects/quantitative-mri.

53. Ostrom, Q. T., Gittleman, H., Fulop, J., Liu, M., Blanda, R., Kromer, C., Wolinsky, Y., Kruchko, C., Barnholtz-Sloan, J. S. (2015): CBTRUS Statistical Report: Primary Brain and Central Nervous System Tumors Diagnosed in the United States in 2008-2012. Neuro Oncol 17 (Suppl 4), iv1-iv62.

54. Panda, A., Chen, Y., Ropella-Panagis, K., Ghodasara, S., Stopchinski, M., Seyfried, N., Wright, K., Seiberlich, N., Griswold, M., Gulani, V. (2019): Repeatability and reproducibility of 3D MR fingerprinting relaxometry measurements in normal breast tissue. J Magn Reson Imaging 50, 1133-1143.

55. Panda, A., Mehta, B. B., Coppo, S., Jiang, Y., Ma, D., Seiberlich, N., Griswold, M. A., Gulani, V. (2017): Magnetic Resonance Fingerprinting-An Overview. Curr Opin Biomed Eng 3, 56-66.

56. Pannese, E. (2011): Morphological changes in nerve cells during normal aging. Brain Struct Funct 216, 85-89.

57. Pell, G. S., Lin, A., Wellard, R. M., Werther, G. A., Cameron, F. J., Finch, S. J., Papoutsis, J., Northam, E. A. (2012): Age-related loss of brain volume and T2 relaxation time in youth with type 1 diabetes. Diabetes Care 35, 513-519.

58. Pierpaoli, C. (2010): Quantitative brain MRI. Top Magn Reson Imaging 21, 63.

59. Pierre, E. Y., Ma, D., Chen, Y., Badve, C., Griswold, M. A. (2016): Multiscale reconstruction for MR fingerprinting. Magn Reson Med 75, 2481-2492.

60. Rodrigue, K. M., Haacke, E. M., Raz, N. (2011): Differential effects of age and history of hypertension on regional brain volumes and iron. Neuroimage 54, 750-759.

61. Schmitt, P., Griswold, M. A., Jakob, P. M., Kotas, M., Gulani, V., Flentje, M., Haase, A. (2004): Inversion recovery TrueFISP: quantification of T(1), T(2), and spin density. Magn Reson Med 51, 661-667.

62. Su, P., Mao, D., Liu, P., Li, Y., Pinho, M. C., Welch, B. G., Lu, H. (2017): Multiparametric estimation of brain hemodynamics with MR fingerprinting ASL. Magnetic Resonance in Medicine 78, 1812-1823.

63. Trattnig, S., Clément, O., de Souza, N., Essig, M., Helbich, T., Kauczor, H. U., Kiessling, F. , Matos, C., Niessen, W., Thoeny, H. C., Vallée, J.-P., van Beek, E., van der Lugt, A., Vilgrain, V. (2015): Magnetic Resonance Fingerprinting - a promising new approach to obtain standardized imaging biomarkers from MRI. Insights Imaging 6, 163-165.

64. Warntjes, J. B., Dahlqvist, O., Lundberg, P. (2007): Novel method for rapid, simultaneous T1, T2*, and proton density quantification. Magn Reson Med 57, 528-537.

65. Warntjes, J. B., Leinhard, O. D., West, J., Lundberg, P. (2008): Rapid magnetic resonance quantification on the brain: Optimization for clinical usage. Magn Reson Med 60, 320-329.

66. Wearn, A. R., Nurdal, V., Saunders-Jennings, E., Knight, M. J., Isotalus, H. K., Dillon, Serena, Tsivos, D., Kauppinen, R. A., Coulthard, E. J. (2020): T2 heterogeneity: a novel marker of microstructural integrity associated with cognitive decline in people with mild cognitive impairment. Alzheimer's Research & Therapy 12, 105.

67. Weigel, M. (2015): Extended phase graphs: dephasing, RF pulses, and echoes - pure and simple. J Magn Reson Imaging 41, 266-295.

68. Weishaupt, D., Koechli, V. D., Marincek, B. (2014): Wie funktioniert MRI? Eine Einführung in Physik und Funktionsweise der Magnetresonanzbildgebung. 7. Ed. Berlin: Springer Verlag.

69. Whittall, K. P., MacKay, A. L., Graeb, D. A., Nugent, R. A., Li, D. K., Paty, D. W. (1997): In vivo measurement of T2 distributions and water contents in normal human brain. Magn Reson Med 37, 34-43.

70. Yu, Z., Zhao, T., Assländer, J., Lattanzi, R., Sodickson, D. K., Cloos, M. A. (2018): Exploring the sensitivity of magnetic resonance fingerprinting to motion. Magn Reson Imaging 54, 241-248.

7. Appendix

7.1 Supplemental material

7.1.1 Comparison of volunteer relaxometry data to conventional mapping techniques

	T_1 and T_2 relaxation times at 1.5 T			
Anatomic region	**Mean T_1** /ms (MRF, present study)	**Mean T_1** /ms (literature)	**Mean T_2** /ms (MRF, present study)	**Mean T_2** /ms (literature)
Frontal white matter	659.18 ± 20.7	556 ± 20 - 756*	40.85 ± 3.04	54 ± 4 - 79 ± 2
Ncl. Caudatus	1046.15 ± 87	1009 ± 48 - 1220*	62.22 ± 3.46	85 ± 2 - 89 ± 6
Putamen	926.36 ± 30.42	832 ± 25 - 1020*	55.21 ± 3.09	75 ± 3 - 81 ± 3
Thalamus	936.14 ± 31.44	738 ± 39 - 975*	54.06 ± 3.46	76 ± 2 - 80 ± 2
C. callosum genu	672.15 ± 53.71	556 ± 38 - 734*	45.48 ± 9.43	71 ± 1 - 76 ± 3
C. callosum splenium	708.62 ± 50.38	567 ± 135 - 778*	48.18 ± 2.33	82 ± 1 - 86 + 5
Frontal gray matter	1086.14 ± 50.95	1048 ± 61 - 1065 ± 51	60.19 ± 5.61	98 ± 7 - 99 ± 4

Table 3: Comparison of MRF-derived mean T_1 and T_2 values plus/minus the standard deviation with quantitative T_1 and T_2 results provided by alternative mapping techniques at 1.5 T which were available in literature (Whittall et al. 1997; Deoni et al. 2005; Lu et al. 2005).
*: No standard deviation presented in corresponding publication

	T_1 and T_2 relaxation times at 3 T			
Anatomic region	**Mean T_1** (MRF, present study)	**Mean T_1** (literature)	**Mean T_2** (MRF, present study)	**Mean T_2** (literature)
Frontal white matter	875.78 ± 28.44	728 ± 433 - 954 ± 39	33.45 ± 2.01	59 ± 4 - 75 ± 3
Ncl. Caudatus	1329.55 ± 39.06	1258 ± 55 - 1483 ± 42	50.71 ± 2.78	59 ± 4 - 69 ± 2
Putamen	1187.15 ± 38.83	1102 ± 40 - 1337 ± 42	43.09 ± 2.26	52 ± 2 - 66 ± 2
Thalamus	1181.56 ± 38.8	986 ± 33 - 1218 ± 40	45.55 ± 2.46	67 ± 2
C. callosum genu	906.28 ± 76.17	721 ± 68	36.18 ± 7.57	65 ± 2
C. callosum splenium	973.14 ± 100.76	748 ± 64	42.06 ± 8.52	75 ± 5
Frontal gray matter	1374.35 ± 62.78	1165 ± 113 - 1615 ± 149	56.55 ± 6.05	71 ± 10 - 110 ± 4

Table 4: Comparison of MRF-derived mean T_1 and T_2 values plus/minus the standard deviation with quantitative T_1 and T_2 results provided by alternative mapping techniques at 3 T which were available in literature (Whittall et al. 1997; Deoni et al. 2005; Bojorquez et al. 2017; Lu et al. 2005)

7.1.2 Comparison of volunteer relaxometry data to previous MRF results

Mean relaxometry values obtained from MRF at 3 T:			
Anatomic region		Mean T_1, T_2 /ms (present study)	Mean T_1, T_2 /ms (Ma et al. 2019)
Centrum semiovale	T_1	920.97 ± 20.46	816.9 ± 24.7
	T_2	44.51 ± 1.45	44.7 ±2.6
Frontal white matter	T_1	875.78 ±28.44	796.9 ± 50.2
	T_2	33.45 ± 2.01	40.2 ±1.5
Nucleus caudatus	T_1	1319.55 ± 39.06	1344.8 ± 69.0
	T_2	50.71 ± 2.78	55.7 ± 2.4
Putamen	T_1	1187.15 ± 38.83	1259.8 ± 41.5
	T_2	43.09 ± 2.26	48.8 ± 2.7
Parietal white matter	T_1	906.16 ± 29.10	816.1 ± 34.0
	T_2	39.78 ± 2.13	43.3 ± 1.7
Cortical gray matter	T_1	1469.26 ± 83.13	1429.8 ± 49.1
	T_2	63.93 ± 7.47	61.9 ± 2.3
Mean relaxometry values obtained from MRF at 1.5 T:			
		Mean T_1, T_2 /ms (present study)	Mean T_1, T_2 /ms (Ma et al. 2013)
White matter (wm)	T_1	659.18 ± 20.7 (frontal wm)	685 ± 33 (unspecified)
	T_2	40.85 ± 3.04 (frontal wm)	65 ± 4 (unspecified)
Gray matter (gm)	T_1	1086.14 ± 50.95 (frontal gm)	1180 ± 104 (unspecified)
	T_2	60.2 ± 5.61 (frontal gm)	97 ± 5.9 (unspecified)

Table 5: Mean T_1 and T_2 relaxation times in different brain tissues measured with MRF from 10 healthy volunteers in comparison with former MRF data available in literature (Ma et al. 2013; Ma et al. 2019).

7.2 List of figures

Figure 1: Sketch of the framework with fundamental elements of the MRF implementation. 11

Figure 2: Overview of the initial MRF acquisition framework. 12

Figure 3: Scheme of the ISMRM/NIST system phantom used for repeated stability MRF scans. 16

Figure 4: T_1 and T_2 maps obtained from MRF scans of the ISMRM system phantom arrays. 22

Figure 5: T_1 and T_2 relaxometry measurements in the ISMRM phantom. 23

Figure 6: Repeatability of the T_1 and T_2 estimates from MRF phantom scans. 24

Figure 7: Correlation- and Bland-Altman plots comparing the T_1 and T_2 values calculated from MRF scans with T_1 and T_2 values derived from NMR inversion recovery spin echo and spin echo methods in the ISMRM phantom. 25

Figure 8: Correlation- and Bland-Altman plots comparing the T_1 and T_2 values calculated from MRF scans with T_1 and T_2 values derived from NMR inversion recovery spin echo and spin echo methods in the ISMRM phantom. 26

Figure 9: T_1 map with reference ROI placement in the upper cranium, mid ventricular and cerebellar level for MRF measurements in healthy volunteers. 28

Figure 10: Box plots from T_1 and T_2 values from 16 different anatomic brain regions obtained by MRF in a total of 10 healthy volunteers. 30

Figure 11: Repeatability of MRF-derived T_1 and T_2 values in 10 healthy volunteers. 31

Figure 12: T_1 map with reference ROI placement in the mid ventricular and cerebellar level for MRF measurements in patient brain. 33

Figure 13: Comparison of T_1 and T_2 measurements from 9 different anatomic brain regions obtained by MRF in a cohort of 92 patients and in 10 healthy volunteers. 35

Figure 14: Comparison of the repeatability of T_1 and T_2 estimates in 9 different anatomic regions from MRF measurements of the entire patient cohort, a sub-group of 10 healthy patients and 10 healthy volunteers. 36

Figure 15: Age dependence of MRF derived T_1 and T_2 values from the frontal matter structure in the patient cohort. 38

7.3 List of tables

Table 1: Age distribution in the patient cohort. 18

Table 2: Total number of T_1 and T_2 values measured per anatomic region from the patient cohort. 33

Table 3: Comparison of MRF-derived mean T_1 and T_2 values with quantitative T_1 and T_2 results provided by alternative mapping techniques at 1.5 T. 54

Table 4: Comparison of MRF-derived mean T_1 and T_2 values with quantitative T_1 and T_2 results provided by alternative mapping techniques at 3 T. 55

Table 5: Mean T_1 and T_2 relaxation times in different brain tissues measured with MRF from 10 healthy volunteers in comparison with former MRF. 56

7.4 List of abbreviations

bSSFP	Balanced steady-state free precession imaging
CPMG	Carr-Purcell-Meiboom-Gill
FA	Flip angle
FID	Free induction decay
FISP	Fast imaging with steady-state free precession
IR-SE	Inversion recovery spin echo
ISMRM	International Society for Magnetic Resonance in Medicine
MRI	Magnetic resonance imaging
MRF	Magnetic resonance fingerprinting
NIST	National Institute of Standards and Technology
NMR	Nuclear magnetic resonance
PPS	Polyphenylene sulfide
RF	Radio frequency
ROI	Region of interest
SQL	Structured query language
T	Tesla
T_1	Longitudinal relaxation time
T_2	Transverse relaxation time
TE	Echo time
TR	Repetition time

8. Acknowledgement

First and foremost, I would like to thank my supervisor Prof. Dr. Lale Umutlu for the opportunity to perform these studies and for her excellent supervision and guidance. I am also greatly thankful to Dr. Marcel Gratz for his supervision and support in experimental, technical and theoretical issues. My sincere gratitude also goes to Privatdozent Dr. Felix Nensa for his tremendous support in informatics. Moreover, I would like to thank Dr. Aydin Demircioglu for his outstanding know-how and support in the statistical analysis.

I am also very grateful for the opportunity to perform measurements on the ISMRM/NIST System phantom kindly supplied by Siemens Healthineers.

9. Curriculum vitae

Der Lebenslauf ist in der Online-Version aus Gründen des Datenschutzes nicht enthalten.